

# A Millimetre Wave Embroidered Antennas

Daggupati Anil Kumar

A Thesis Submitted to  
Indian Institute of Technology Hyderabad  
In Partial Fulfillment of the Requirements for  
The Degree of Master of Technology

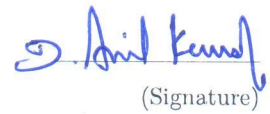


Department of Electrical Engineering

June 2018

## Declaration

I declare that this written submission represents my ideas in my own words, and where ideas or words of others have been included, I have adequately cited and referenced the original sources. I also declare that I have adhered to all principles of academic honesty and integrity and have not misrepresented or fabricated or falsified any idea/data/fact/source in my submission. I understand that any violation of the above will be a cause for disciplinary action by the Institute and can also evoke penal action from the sources that have thus not been properly cited, or from whom proper permission has not been taken when needed.

  
(Signature)

---

(Daggupati Anil Kumar)

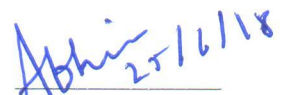
EE16MTECH11002  
(Roll No.)

## Approval Sheet

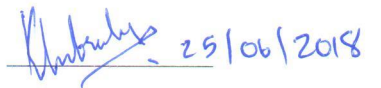
This Thesis entitled A Millimetre Wave Embroidered Antennas by Daggupati Anil Kumar is approved for the degree of Master of Technology from IIT Hyderabad



Prof. Mohammed Zafar Ali Khan  
Adviser  
Dept. of Electrical Engineering  
IIT Hyderabad



Dr. Abhinav Kumar  
Internal Examiner  
Dept. of Electrical Engineering  
IIT Hyderabad



Dr. Subrahmanyam Kalyanasundaram  
External Examiner  
Dept. of Computer Science Engineering  
IIT Hyderabad

## Acknowledgements

I would like to express my sincere gratitude to my guide **Dr. Mohammed Zafar Ali Khan** for the continuous support of my 2 year research work, for his motivation, patience and immense knowledge. His expertise, invaluable guidance, encouragement and affectionate attitude added considerably to my experience.

# Dedication

Dedicated to my parents

## **Abstract**

WLAN and Body Area Networks(BAN) are rapidly advancing as high data rate wireless communication systems using Ultra Wide Band(UWB) spectrum. The unlicensed UWB spectrum offers 7 GHz wide bandwidth which ranges over 57 to 64 GHz. In this UWB communication systems Antenna design plays a crucial role for signal transmission and reception. However Antenna design at UWB spectrum is more challenging than narrow band design Beam forming Antenna arrays play an important role at these frequencies. In this work A novel embroidery type dipole antennas and dipole arrays are proposed for Body area networks. The proposed antennas are designed and analyzed using High Frequency Structure Simulator(HFSS).

# Contents

Declaration . . . . .	ii
Approval Sheet . . . . .	iii
Acknowledgements . . . . .	iv
Abstract . . . . .	vi
<b>Nomenclature</b>	<b>viii</b>
<b>1 Introduction</b>	<b>1</b>
1.1 UWB Spectrum and Millimetre Waves . . . . .	1
1.2 Body Centric Communications . . . . .	2
1.2.1 Off-body communications . . . . .	2
1.2.2 On-body communications . . . . .	2
1.2.3 In-body communications . . . . .	2
1.3 Wearable Antennas at Millimeter Waves . . . . .	3
1.4 Literature and Contributions . . . . .	4
<b>2 Multiturn Millimetre Full-wave Dipole Antenna</b>	<b>5</b>
2.1 Antenna Design . . . . .	5
2.2 Current Distribution . . . . .	6
2.2.1 Antenna Parameterization . . . . .	6
2.3 Far-field calculation . . . . .	6
2.3.1 Magnetic vector potential . . . . .	7
2.3.2 Magnetic and Electric field calculation . . . . .	10
2.3.3 Theoretical and Simulation Results . . . . .	11
<b>3 Dipole Antenna with N Turns</b>	<b>15</b>
3.1 Introduction . . . . .	15
3.2 $3\frac{\lambda}{2}$ Dipole antenna . . . . .	15
3.3 $4\frac{\lambda}{2}$ Dipole antenna . . . . .	19
3.4 $5\frac{\lambda}{2}$ Dipole antenna . . . . .	21
3.5 $6\frac{\lambda}{2}$ Dipole antenna . . . . .	23
3.6 $7\frac{\lambda}{2}$ Dipole antenna . . . . .	24
3.7 $8\frac{\lambda}{2}$ Dipole antenna . . . . .	26
3.8 Conclusion . . . . .	27

<b>4</b>	<b>Millimetre wave Embroidery Beamforming Antenna arrays</b>	<b>28</b>
4.1	Introduction . . . . .	28
4.2	Antenna Array setup . . . . .	28
4.3	Antenna array with Reflector . . . . .	29
4.4	Antenna Parameters . . . . .	29
4.4.1	Directivity and Gain . . . . .	29
4.4.2	Radiated Electric field . . . . .	29
4.4.3	Return losses and Mutual coupling . . . . .	31
4.4.4	Antenna feeding and impedance Matching . . . . .	31
4.5	Limitation on number of Antenna Elements and length . . . . .	34
4.6	Conclusion and Future work . . . . .	34
	<b>References</b>	<b>36</b>
<b>A</b>	<b>High Frequency Structure Simulator</b>	<b>39</b>
A.1	Introduction . . . . .	39
A.2	Mathematical method used by HFSS . . . . .	39
A.2.1	Adaptive solution . . . . .	39
A.3	Steps followed in HFSS simulation . . . . .	41
A.4	Materials and Dimensions . . . . .	42



# Chapter 1

## Introduction

### 1.1 UWB Spectrum and Millimetre Waves

The unlicensed ultra-wide band spectrum 57-64GHz which has 7GHz bandwidth is used for short distance communication [1, 2]. The millimetre waves in this band have high attenuation due to oxygen and water content present in the atmosphere. Approximately the attenuation for this band is 12-15 dB/Km and penetration through concrete walls is negligible due to huge amount of power loss. So this high attenuation enables more secure communication and is most suitable for indoor communication. we get low interference with other frequency channels in this spectrum and it enables frequency reuse in adjacent wireless networks [3].

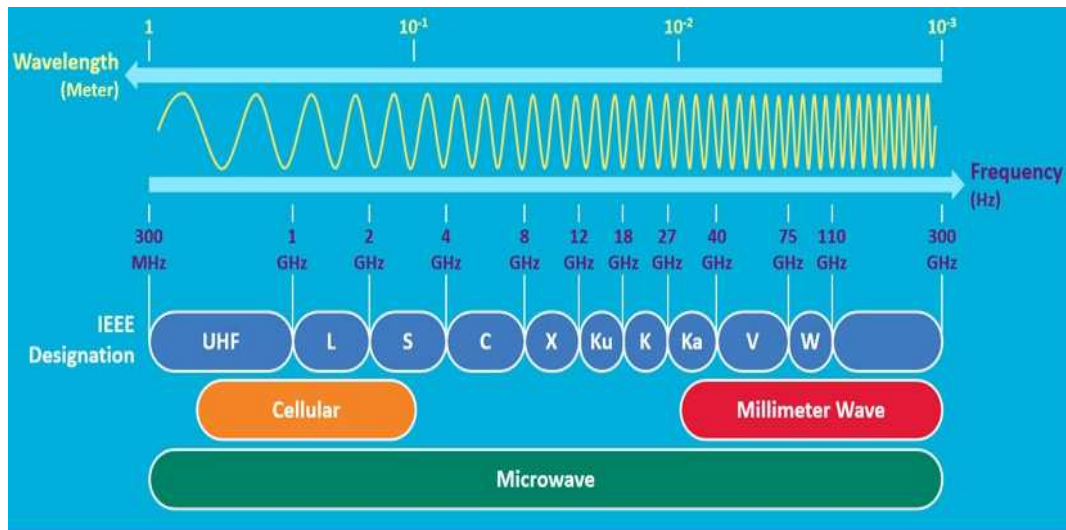


Figure 1.1: Millimetre wave band in spectrum [4]

The UWB 60GHz band can achieve gigabit per second data rates for short range wireless communications because of availability of huge bandwidth. Because of these advantages millimetre waves created research interests and their practical applications. Figure 1.1 shows FCC frequency allotted bands [5] where as our interested frequency range is in the V band.

## 1.2 Body Centric Communications

Body centric wireless communication is one of the fast growing technologies. It is important in 4th generation and beyond wireless communication systems. As time progress due to advanced technology in wireless communications, minimization of wearable hardware, embedded software and digital signal processing has enabled us human to human networking by incorporating wearable sensors and communications [6],[7],[8]. This Body centric communication technology using in different occupations like paramedics, military, fire fighters and health-care. The wearable systems has high importance on computational power when we coupled with sensors and interface components. But these systems are bulky and have wired connections. The wireless communications in this systems have highly desirable.

Body centric communications consists of Body Area Networks(BAN) and Personal Area Networks(PAN). The content of PAN or BAN contains a range of communication requirements. These are classified into 3 types [6].

- Off-body communications
- On-body communications
- In-body communications

### 1.2.1 Off-body communications

The radio wireless communications dealing this type of off-body communications like human to human, human to base station communications.

### 1.2.2 On-body communications

On-body communication system design is most important and challenging because several factors are involved in this design. There are several devices carried by human which need to communicate with each other. The choice of frequency of operation in wearable devices is also desirable because at low frequencies wave length is high and penetration depth to human body is also high [9]. They effect human body When penetrated into the body. Most of previous studies for on-body communications conducted at microwave frequencies like 2.4GHz and 4.5GHz, wearable devices operated at microwaves are large when compared to 60GHz ultra wide band and we achieve high data rates. Figure 1.2 depicts the soldier on-body communication in the battle field. In this figure (1,2,3,4,5) are the sensors carried by soldier in battle field [10].

### 1.2.3 In-body communications

One of the applications in wireless body area networks is health-care. Millimetre wave technology enables long term patient monitoring for health problems by using wearable devices and in-planted body sensors with out disturbing the human daily activities. In this RF communication system wearable antenna design is challenging. The data which is collected by all the sensors placed in/on the human body is of high importance. Hence we need to transmit it to base station properly with out errors. So wearable antenna design has great importance. Millimetre wave interactions with the human body are discussed in [11, 12].

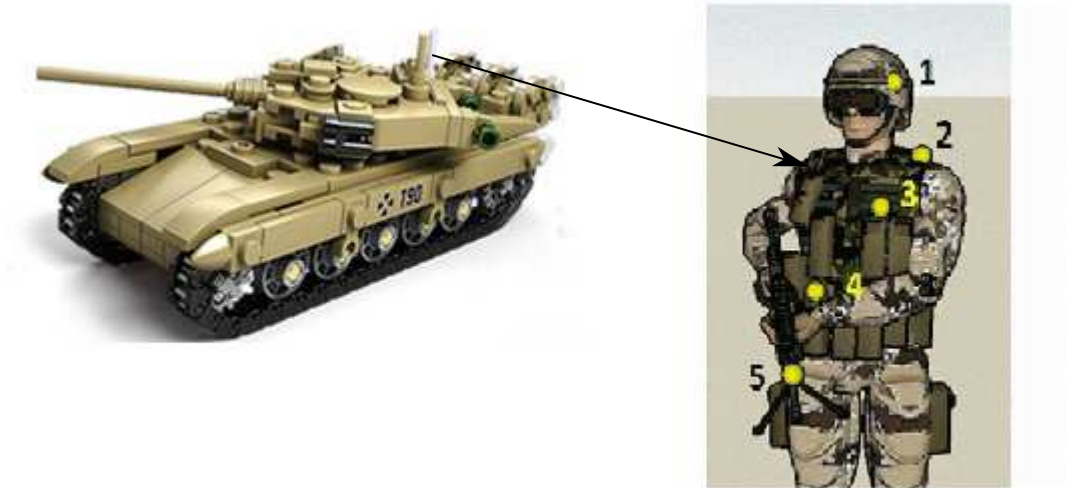


Figure 1.2: Communication between base station and soldier [13]

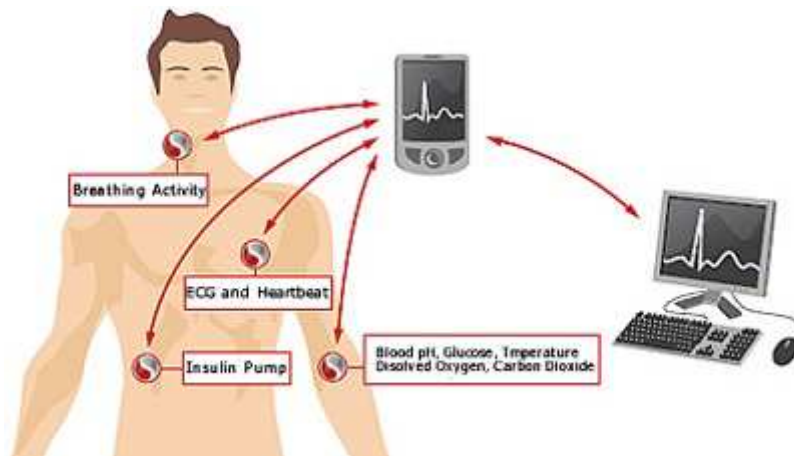


Figure 1.3: Patient health monitoring [14]

### 1.3 Wearable Antennas at Millimeter Waves

Wearable antenna is defined as an antenna to be a part of clothing. It is clear that antennas are worn on the body placed in the equipment which are attached to the body directly such as soldier equipment and medical sensors as discussed in the above section. Due to high importance to wearable antennas researchers also interest in that designs. The wavelength at ultra wide bandwidth i.e. 60GHz is 5mm. Designing wearable antennas at millimeter wavelength is challenging. The existing wearable antennas are prone to

- Bending
- Flexing
- Wrinkling

So wearable antennas need to be unchanged and operational at above circumstances. Earlier in this area a lot of antenna designs for various operating frequency are proposed and practically designed. Designs like planar inverted antennas [15] for GSM wearable applications, Yagi-uda [16] and micro strip patch antennas [17] at 60GHz are designed but these antennas are not the part of clothes. In this work the proposed antenna designs are easy to fabric and the designs overcome above mentioned challenges. The design has advantage like easy to fabric.

## 1.4 Literature and Contributions

Key aspect for this proposed antenna is it should be easily embroidered on clothes. The basic half-wave dipole antenna is designed in the paper [18] where dipole construction, Theoretical far-field mathematical expressions and simulation results are discussed.

The proposed structure in [18] is gives us advantage to easily embroider on clothes because of curved shapes. But the problem is length of the antenna, at this frequency of operation (60GHz) half-wavelength(2.5mm) which is difficult to embroider on clothes, length is not long enough to stick on clothes.

So we consider the problem of increased length of the antenna i.e. increase sufficient number of turns to embroidery on cloth and it should be flexible. In this work we designed symmetric full-wave dipole antenna with respect to antenna feed point. Antenna construction details and far field expressions are discussed in chapter 3 and published in [19]. In this design we focus on current distribution on antenna and far-field mathematical expressions. The design is simulated using High Frequency Structure Simulator(HFSS) which is discussed in appendix. There is good matching between theoretical and simulated far-field results.

As length of the antenna increase symmetrically, finding mathematical expressions for far-field becomes difficult. So we observed the far-fields around the antenna by simulating in HFSS for different lengths. These results are discussed in the chapter 3.

So far we have discussed only dipoles. They radiate in all directions, directivity and gain of single antenna for communication is low at these operating frequency(60GHz). So we need to design antenna arrays for getting strong and highly directive beams. We proposed a novel embroidered antenna design in chapter 4. The main aim of this array design is to steer beams in required direction so we analyzed different types of arrays. We proposed broadside embroidery array [20]. In the array design disadvantage is side-lobe power, radiated power is wasted in terms of side-lobes. So we need to reduce the side-lobe effect and strengthen the main beams. To ensure that in this array design we observed field patterns with different antenna element combinations and different feeding phases. After several observations we recommended  $N=8$  antenna elements and each antenna element length is  $7\frac{\lambda}{2}$  with these specification we got highly directional and high gain beams. The complete details discussed in chapter 4.

## Chapter 2

# Multiturn Millimetre Full-wave Dipole Antenna

### 2.1 Antenna Design

The geometry of proposed antenna consists of four semi circular arms to make sure that the length of antenna is full wavelength i.e. 5mm. Length of each arm is  $\frac{\lambda}{4}$  such that total length is  $\lambda$ . Antenna is positioned along YZ axis symmetrically as shown in Figure 2.1. The basic construction details of multiturn antenna discussed in [18, 21]. Feeding point for the antenna is center point as shown in the Figure 2.1. We can select off-center feed point and make sure that current at that point is not equal to zero.

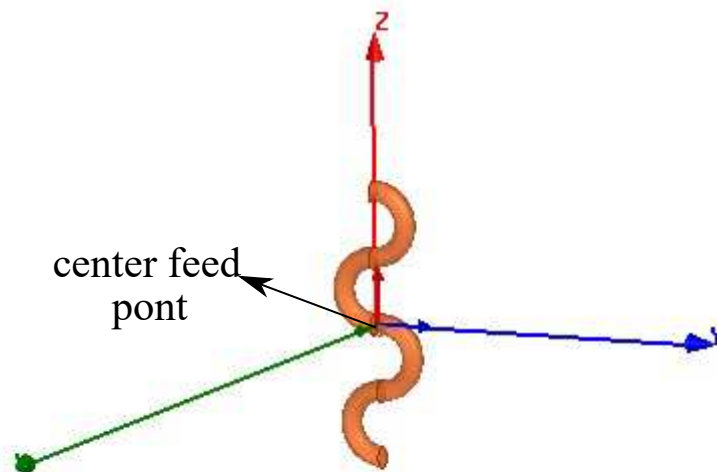


Figure 2.1: Full-wave Dipole Antenna

## 2.2 Current Distribution

For the proposed antenna we assumed the current distribution is sinusoidal [22]. the following equation is represents current distribution. In Equation 2.1  $k$  is wave-number,  $H$  is half length of antenna i.e.  $\frac{\lambda}{2}$  where  $\lambda$  is wavelength of dipole.

$$I(Z) = I_O \sin \left( k(H - |Z|) \right), \quad (2.1)$$

### 2.2.1 Antenna Parameterization

For calculating the far-field equations of proposed antenna, the antenna geometry is parameterized by  $t$  which varies from  $-\pi$  to  $\pi$ . The geometry of four arms of the dipole and their respective tangents are defined by following vector expressions.

*Arm - 1*

$$l_1 = \hat{a}_y v \sin t + \hat{a}_z (3v + v \cos t); \quad -2\pi \leq t \leq -\pi$$

$$\hat{T}_1 = \hat{a}_y \cos t - \hat{a}_z \sin t.$$

*Arm - 2*

$$l_2 = \hat{a}_y v \sin t + \hat{a}_z (v - v \cos t); \quad -\pi \leq t \leq 0$$

$$\hat{T}_2 = \hat{a}_y \cos t + \hat{a}_z \sin t.$$

*Arm - 3*

$$l_3 = \hat{a}_y v \sin t + \hat{a}_z (-v + v \cos t); \quad 0 \leq t \leq \pi$$

$$\hat{T}_3 = \hat{a}_y \cos t - \hat{a}_z \sin t.$$

*Arm - 4*

$$l_4 = \hat{a}_y v \sin t + \hat{a}_z (-3v - v \cos t); \quad \pi \leq t \leq 2\pi$$

$$\hat{T}_4 = \hat{a}_y \cos t + \hat{a}_z \sin t.$$

(2.2)

For the proposed antenna current distribution is sinusoidal and it's direction is tangential to curve [23, 22]. The current equations for each arm is given by

$$I_1 = I_O \sin (\pi + |kvt|) \hat{a}_y \cos t - \hat{a}_z \sin t,$$

$$I_2 = I_O \sin (\pi + |kvt|) \hat{a}_y \cos t + \hat{a}_z \sin t,$$

$$I_3 = I_O \sin (\pi + |kvt|) \hat{a}_y \cos t - \hat{a}_z \sin t,$$

$$I_4 = I_O \sin (\pi + |kvt|) \hat{a}_y \cos t + \hat{a}_z \sin t,$$

(2.3)

Where  $I_O$  is the peak value of the current, and current has no component along x-axis, and  $\hat{a}_y$ ,  $\hat{a}_z$  are unit vectors along Y and Z directions. Note that the current is zero at both the ends of the antenna.

## 2.3 Far-field calculation

Field around the antenna can be divided in to three regions.

- Reactive Near field
- Radiating Near field
- Radiating far-field

The near field and reactive field are die off with distances as  $\frac{1}{R^2}$  and  $\frac{1}{R^3}$ , where  $\mathbf{R}$  is the observing point from the antenna [22]. So we are left with Radiating far-fields, in this region radiation patters does not change with distance. This region is one of the most important region, it determines the antenna radiation pattern. This is the region which is operating region of antenna. So to calculate the radiated Electric and Magnetic fields in this region we can follow two step procedure as discussed in [22]. In this procedure first Magnetic vector potential  $\mathbf{A}$  is calculated then Electric  $\mathbf{E}$  and Magnetic field  $\mathbf{H}$  are calculated.

### 2.3.1 Magnetic vector potential

$\mathbf{A}$  can be calculated as

$$\mathbf{A}(X, Y, Z) = \frac{\mu}{4\pi} \int_c I_{arm}(X', Y', Z') \frac{e^{jkR}}{R} dl' \quad (2.4)$$

Where  $\mu$  is permeability, point  $(X', Y', Z')$  is the source point and the point  $(X, Y, Z)$  is the observation point. The relation between source and observation point is

$$R = \sqrt{(X' - X)^2 + (Y' - Y)^2 + (Z' - Z)^2} \quad (2.5)$$

source coordinates  $(X', Y', Z')$  are parameterized by parameter  $t$  and observation point is in spherical coordinate system. so we have

$$\begin{aligned} X' = 0, Y' = v \sin t, Z' = 3v + v \cos t; & \quad -2\pi \leq t \leq -\pi \\ X' = 0, Y' = v \sin t, Z' = -v - v \cos t; & \quad -\pi \leq t \leq 0 \\ X' = 0, Y' = v \sin t, Z' = -v + v \cos t; & \quad 0 \leq t \leq \pi \\ X' = 0, Y' = v \sin t, Z' = -3v - v \cos t; & \quad \pi \leq t \leq 2\pi \end{aligned} \quad (2.6)$$

$$\begin{aligned} X &= r \sin \theta \cos \phi, \\ Y &= r \sin \theta \sin \phi, \\ Z &= r \cos \theta. \end{aligned} \quad (2.7)$$

Where point  $(r, \theta, \phi)$  is the observation point in the spherical coordinate system. From (2.3) we can observe that the current has two components along  $\mathbf{y}$  and  $\mathbf{z}$  directions. So the magnetic field vector exists only in  $\mathbf{y}$  and  $\mathbf{z}$  directions,  $A_y$  and  $A_z$ . The corresponding expressions are

$$\begin{aligned} A_y &= A_{y1} + A_{y2} + A_{y3} + A_{y4}, \\ A_z &= A_{z1} + A_{z2} + A_{z3} + A_{z4}. \end{aligned} \quad (2.8)$$

Each integration in (3.8) is solved by using Simpson's  $\frac{3^{th}}$  rule, and the expressions are given by

$$A_{y1} = \frac{\mu v I_O \exp(-jkr)}{4\pi r} \int_{-2\pi}^{-\pi} \left( \sin(kH - |kvt|) \cos t \right. \\ \left. \times \exp(-jk(-v \sin \theta \sin \phi \sin t - v(3 + \cos t) \cos \theta)) \right) dt, \quad (2.9)$$

by this Simpson's rule

$$A_{y1} \approx K \left[ \exp(-j\frac{1}{4}(-\sqrt{3} \sin \theta \sin \phi - 7 \cos \theta)) - \sqrt{3} \exp(-j\frac{1}{4}(-\sqrt{3} \sin \theta \sin \phi - 5 \cos \theta)) - \frac{4}{3} \exp(j \cos \theta) \right], \quad (2.10)$$

In a similar manner

$$A_{y2} = \frac{\mu v I_O \exp(-jkr)}{4\pi r} \int_{-\pi}^0 \left( \sin(kH - |kvt|) \cos t \right. \\ \left. \times \exp(-jk(-v \cos \theta \sin \theta \sin t - v \cos \theta(1 - \cos t))) \right) dt, \quad (2.11)$$

$$A_{y2} \approx K \left[ -\sqrt{3} \exp(-j\frac{1}{4}(\sqrt{3} \sin \theta \sin \phi - 3 \cos \theta)) + \exp(-j\frac{1}{4}(\sqrt{3} \sin \theta \sin \phi - \cos \theta)) - \frac{4}{3} \exp(j \cos \theta) \right], \quad (2.12)$$

and

$$A_{y3} = \frac{\mu v I_O \exp(-jkr)}{4\pi r} \int_0^{\pi} \left( \sin(kH - |kvt|) \cos t \right. \\ \left. \times \exp(-jk(-v \sin \theta \sin \phi \sin t + v \cos \theta(1 - \cos t))) \right) dt, \quad (2.13)$$

$$A_{y3} \approx K \left[ \exp(-j\frac{1}{4}(-\sqrt{3} \sin \theta \sin \phi + \cos \theta)) - \sqrt{3} \exp(-j\frac{1}{4}(-\sqrt{3} \sin \theta \sin \phi + 3 \cos \theta)) - \frac{4}{3} \exp(j \cos \theta) \right], \quad (2.14)$$

$$A_{y4} = \frac{\mu v I_O \exp(-jkr)}{4\pi r} \int_{\pi}^{2\pi} \left( \sin(kH - |kvt|) \cos t \right. \\ \left. \times \exp(-jk(-v \sin \theta \sin \phi \sin t + v(3 + \cos t) \cos \theta)) \right) dt, \quad (2.15)$$

$$A_{y4} \approx K \left[ -\sqrt{3} \exp(-j\frac{1}{4}(\sqrt{3} \sin \theta \sin \phi + 5 \cos \theta)) + \exp(-j\frac{1}{4}(\sqrt{3} \sin \theta \sin \phi + 7 \cos \theta)) - \frac{4}{3} \exp(j \cos \theta) \right], \quad (2.16)$$



From equation (3.10),(3.12),(3.14) and (3.16) we can write the final  $A_y$  as

$$A_y = -K \left[ 2\sqrt{3} \cos \left( \frac{1}{4} \left( \sqrt{3} \sin \theta \sin \phi + 5 \cos \theta \right) \right) - 2 \cos \left( \frac{1}{4} \left( \sqrt{3} \sin \theta \sin \phi + 7 \cos \theta \right) \right) \right. \\ \left. + 2\sqrt{3} \cos \left( \frac{1}{4} \left( \sqrt{3} \sin \theta \sin \phi - 3 \cos \theta \right) \right) - 2 \cos \left( \frac{1}{4} \left( \sqrt{3} \sin \theta \sin \phi - \cos \theta \right) \right) + \frac{16}{3} \cos(\cos \theta) \right]. \quad (2.17)$$

Similarly  $A_z$  can be approximated as

$$A_{z1} \approx K \left[ -\sqrt{3} \exp(-j\frac{1}{4}(-\sqrt{3} \sin \theta \sin \phi - 7 \cos \theta)) \right. \\ \left. + 3 \exp(-j\frac{1}{4}(-\sqrt{3} \sin \theta \sin \phi - 5 \cos \theta)) \right] \quad (2.18)$$

$$A_{z2} \approx K \left[ -3 \exp(-j\frac{1}{4}(\sqrt{3} \sin \theta \sin \phi - 3 \cos \theta)) \right. \\ \left. - \sqrt{3} \exp(-j\frac{1}{4}(\sqrt{3} \sin \theta \sin \phi - \cos \theta)) \right] \quad (2.19)$$

$$A_{z3} \approx K \left[ -\sqrt{3} \exp(-j\frac{1}{4}(-\sqrt{3} \sin \theta \sin \phi + \cos \theta)) \right. \\ \left. - 3 \exp(-j\frac{1}{4}(-\sqrt{3} \sin \theta \sin \phi + 3 \cos \theta)) \right] \quad (2.20)$$

$$A_{z4} \approx K \left[ -3 \exp(-j\frac{1}{4}(\sqrt{3} \sin \theta \sin \phi + 5 \cos \theta)) \right. \\ \left. - \sqrt{3} \exp(-j\frac{1}{4}(\sqrt{3} \sin \theta \sin \phi + 7 \cos \theta)) \right] \quad (2.21)$$

From equations (3.18),(3.19),(3.20) and (3.21) we can write the final  $A_z$  as

$$A_z = -K \left[ 6 \cos \left( \frac{1}{4} \left( \sqrt{3} \sin \theta \sin \phi + 5 \cos \theta \right) \right) + 2\sqrt{3} \cos \left( \frac{1}{4} \left( \sqrt{3} \sin \theta \sin \phi + 7 \cos \theta \right) \right) \right. \\ \left. + 6 \cos \left( \frac{1}{4} \left( \sqrt{3} \sin \theta \sin \phi - 3 \cos \theta \right) \right) + 2\sqrt{3} \cos \left( \frac{1}{4} \left( \sqrt{3} \sin \theta \sin \phi - \cos \theta \right) \right) \right]. \quad (2.22)$$

Converting rectangular to spherical coordinates

$$A_r = A_Y \sin \theta \sin \phi + A_Z \cos \theta, \\ A_\theta = A_Y \sin \theta \sin \phi - A_Z \sin \theta, \\ A_\phi = A_Y \cos \phi. \quad (2.23)$$

Hence the expressions for  $A_r$ ,  $A_\theta$  and  $A_\phi$  can be written as

$$\begin{aligned}
A_r &= K \left[ 2\sqrt{3}\cos(a_1) - 2\cos(a_2) + 2\sqrt{3}\cos(a_3) - 2\cos(a_4) + \frac{16}{3}\cos(\cos\theta) \right] \\
&\quad \sin\theta \sin\phi + K \left[ 6\cos(a_1) + 2\sqrt{3}\cos(a_2) + 6\cos(a_3) + 2\sqrt{3}\cos(a_4) \right] \cos\theta, \\
A_\theta &= K \left[ 2\sqrt{3}\cos(a_1) - 2\cos(a_2) + 2\sqrt{3}\cos(a_3) - 2\cos(a_4) + \frac{16}{3}\cos(\cos\theta) \right] \\
&\quad \cos\theta \sin\phi - K \left[ 6\cos(a_1) + 2\sqrt{3}\cos(a_2) + 6\cos(a_3) + 2\sqrt{3}\cos(a_4) \right] \sin\theta, \\
A_\phi &= K \left[ 2\sqrt{3}\cos(a_1) - 2\cos(a_2) + 2\sqrt{3}\cos(a_3) - 2\cos(a_4) + \frac{16}{3}\cos(\cos\theta) \right] \cos\theta.
\end{aligned} \tag{2.24}$$

where  $a_1, a_2, a_3, a_4$  and  $K$  are given by

$$\begin{aligned}
a_1(\theta, \phi) &= \frac{\sqrt{3}\sin\theta \sin\phi + 5\cos\theta}{4}, \\
a_2(\theta, \phi) &= \frac{\sqrt{3}\sin\theta \sin\phi + 7\cos\theta}{4}, \\
a_3(\theta, \phi) &= \frac{\sqrt{3}\sin\theta \sin\phi - 3\cos\theta}{4}, \\
a_4(\theta, \phi) &= \frac{\sqrt{3}\sin\theta \sin\phi - \cos\theta}{4}, \\
K &= \frac{3\pi\mu\nu I_O \exp(-jkr)}{128\pi r}.
\end{aligned} \tag{2.25}$$

### 2.3.2 Magnetic and Electric field calculation

We can calculate the Magnetic field  $\mathbf{H}$  from the following Equation

$$H = \frac{1}{\mu} \Delta \times A \tag{2.26}$$

In the spherical coordinate system,  $\mathbf{H}$  field has three components along  $r, \theta$  and  $\phi$  directions. in far field region, since  $r > \lambda$ ,  $\frac{1}{r^n}$  terms neglected where  $n \geq 2$ . The Final calculated expressions are

$$H_r \approx 0, \tag{2.27}$$

$$H_\theta = \frac{jk}{\mu} A_\phi, \tag{2.28}$$

$$H_\phi = \frac{-jk}{\mu} A_\theta, \tag{2.29}$$

The  $\mathbf{E}$  field is obtained by considering far field approximations, so that

$$E = \frac{1}{j\omega\epsilon} \Delta \times H, \tag{2.30}$$

$$E_r \approx 0, \tag{2.31}$$

$$E_\theta = \frac{K^2}{j\omega\mu\epsilon} A_\theta, \tag{2.32}$$

$$E_\phi = \frac{-k^2}{j\omega\mu\epsilon} A_\phi, \quad (2.33)$$

The total electric field can be written as

$$E_T = \sqrt{E_\theta^2 + E_\phi^2}. \quad (2.34)$$

### 2.3.3 Theoretical and Simulation Results

In this section we find out the antenna parameters like Power density, Radiation intensity, Input and radiation resistance and Directivity.

#### Power density

From the average Poynting vector, we have

$$W_{avg} = \frac{1}{2} \text{Re} [E \times H^*] = \frac{\hat{a}_r}{2\eta} [|E_\theta|^2 + |E_\phi|^2] \quad (2.35)$$

from (36),(38) we can write power density as

$$W_{avg} = \frac{\hat{a}_r \cdot \eta k^2}{2\mu^2} [|A_\theta|^2 + |A_\phi|^2]. \quad (2.36)$$

#### Radiation intensity

The radiation intensity given by

$$U = r^2 W_{avg} \quad (2.37)$$

We can calculate the radiated power by integrating the power density over sphere radius r

$$\begin{aligned} P_{rad} &= \int_0^{2\pi} \int_0^\pi W_{avg} \cdot \hat{a}_r r^2 \sin\theta d\theta d\phi \\ P_{rad} &= \frac{\eta}{2} |I_0|^2 \left( \frac{3kv}{64} \right)^2 (C) \end{aligned} \quad (2.38)$$

where C=801.24.

#### Input and Radiation Resistance

The input impedance of an antenna is defined as the impedance offered by antenna at its input terminals. Input impedance is a complex quantity. Real part of input impedance is the input resistance. Radiation resistance is same as input resistance for loss-less antenna and is related to total radiated real power. 2.3 represents the Impedance plot of the proposed antenna by using HFSS.

$$P_{rad} = \frac{|I_0|^2}{2} R_{rad} R_{rad} = \frac{2P_{rad}}{|I_0|^2} \quad (2.39)$$

the value of Radiation Resistance calculated approximately

$$R_{rad} = 165.9\Omega \quad (2.40)$$

## Directivity

Directivity of an antenna is defined as the ratio of the radiation intensity in a given direction to the radiation intensity averaged over all directions. For proposed antenna the direction of maximum radiation intensity is at an elevation angle of  $110^\circ$ , and directivity  $D_O \approx 1.72$ .

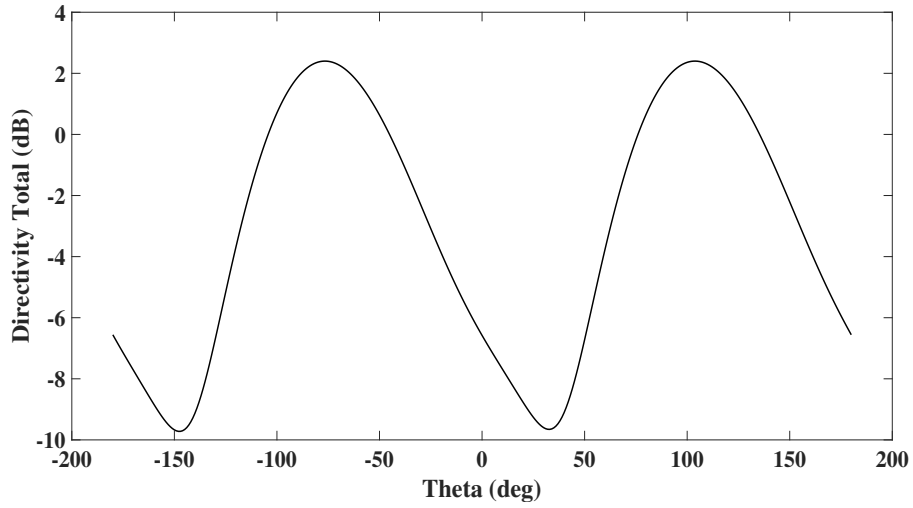


Figure 2.2: Directivity plot of Proposed Antenna

## Antenna feeding and impedance matching

The center fed antenna shown in Figure 2.1. we can select the off-centre feed point along the antenna to make sure that current will not be equal to zero at feed point, and radiation pattern of the antenna follow as half wave dipole antenna.

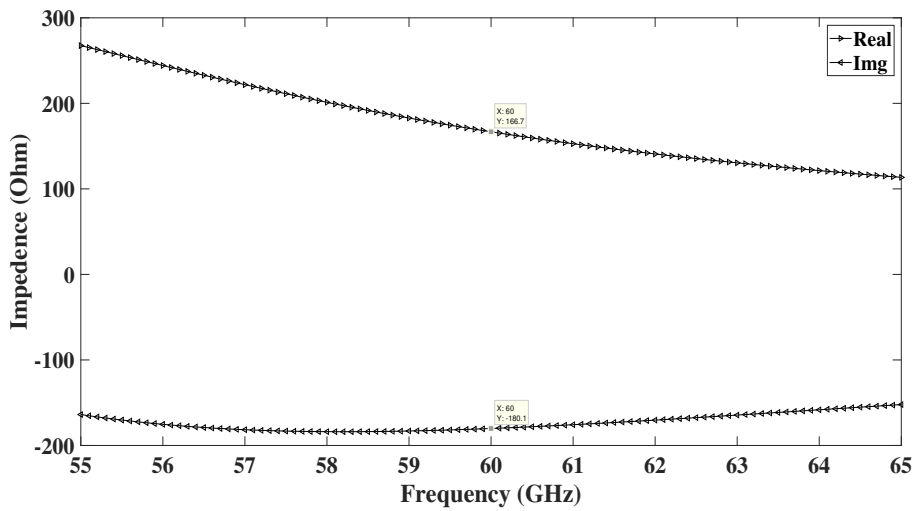


Figure 2.3: Impedance plot of Proposed Antenna

When we observe the radiation resistance from Section III,  $R_{rad} = 165.9\Omega$ .  $R_{rad}$  is approximately

equal to real part of input impedance of the antenna shown in Figure 2.3 It is found that input impedance has reactance component as  $180\omega$ . For the antenna resonance we need to match the input impedance with suitable matching components between the load (antenna) and excitation.

We can use single stub matching to match the antenna[24] impedance by selecting proper coaxial cable. In this work we selected  $125\Omega$  characteristic impedance coaxial cable. Short circuited stubs are preferable than open circuited stubs. Using Smith chart,

$$\begin{aligned} \text{length of stub (l)} &= 0.106\lambda \\ &= 0.265\text{mm}, \\ \text{location of stub from load (d)} &= 0.105\lambda \\ &= 0.263\text{mm}. \end{aligned} \quad (2.41)$$

### Simulation Results

In this section theoretical expressions are verified with simulation results by using HFSS. To make the antenna resonant with reduced reactive component we reduced the antenna size as in[18]. Here we took antenna length as  $0.8\lambda$  instead of full wavelength( $\lambda$ ), so that current not equal to zero at the feed point.

The E field is given by (3.34), which was plotted using MATLAB is shown in Figure 2.4(a). The Radiation pattern obtained using theoretical expressions the dipole has maximum gain at  $110^\circ$ . Figure 2.4(b) shows the radiation pattern of the simulated antenna which has maximum at  $103^\circ$  which is a close match with the theoretically obtained value.

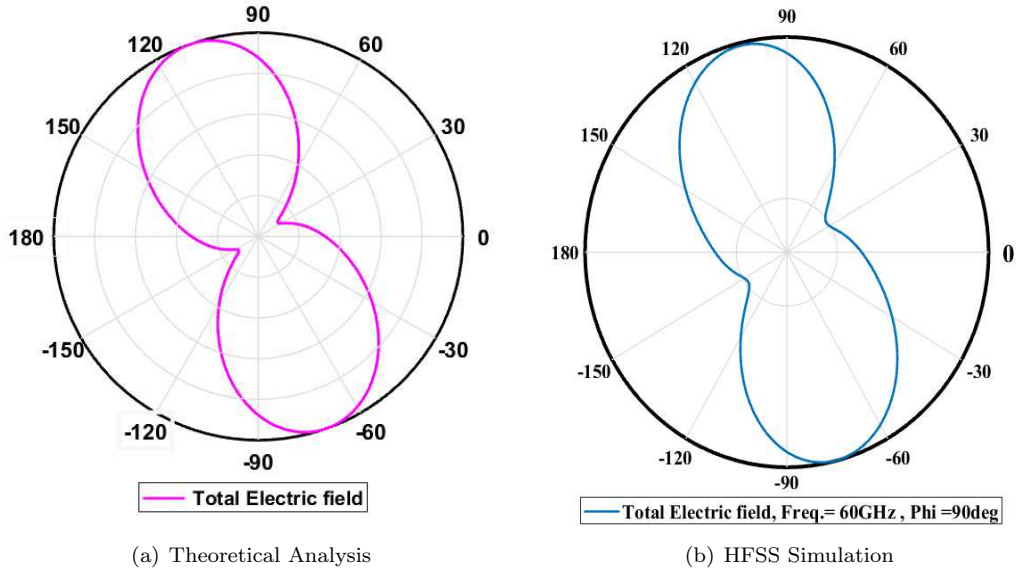


Figure 2.4: Total Electric field comparison

The return loss of proposed antenna shown in Figure 2.6, antenna resonates at 60GHz and covers the entire unlicensed ultra-wide band from 57 GHz to 64 GHz. To verify directivity found using theoretical analysis, directivity plotted using HFSS. Theoretical directivity is 1.72 at an elevation angle  $110^\circ$  where as in simulation 2.4 dB obtained at an elevation angle  $103^\circ$ . The 2D

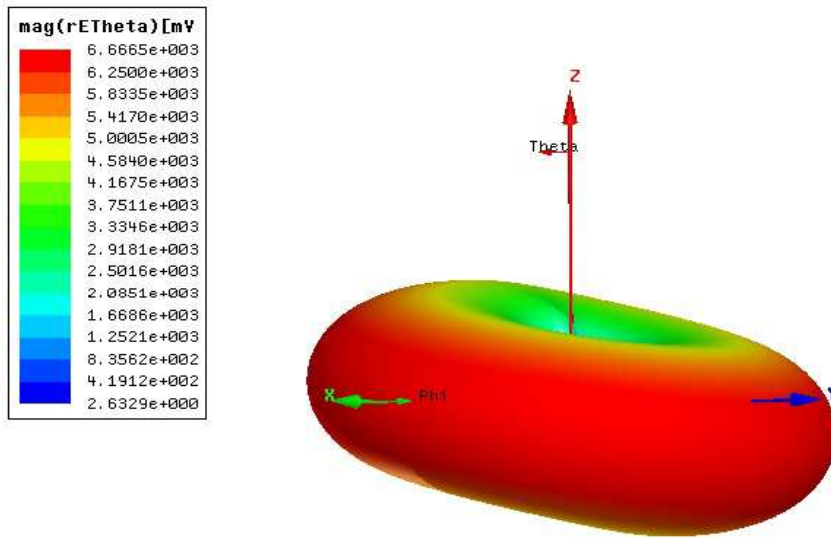


Figure 2.5: 3D Radiation Pattern

plot of directivity is given in Fig.5. The impedance at resonance is shown in Fig.6.

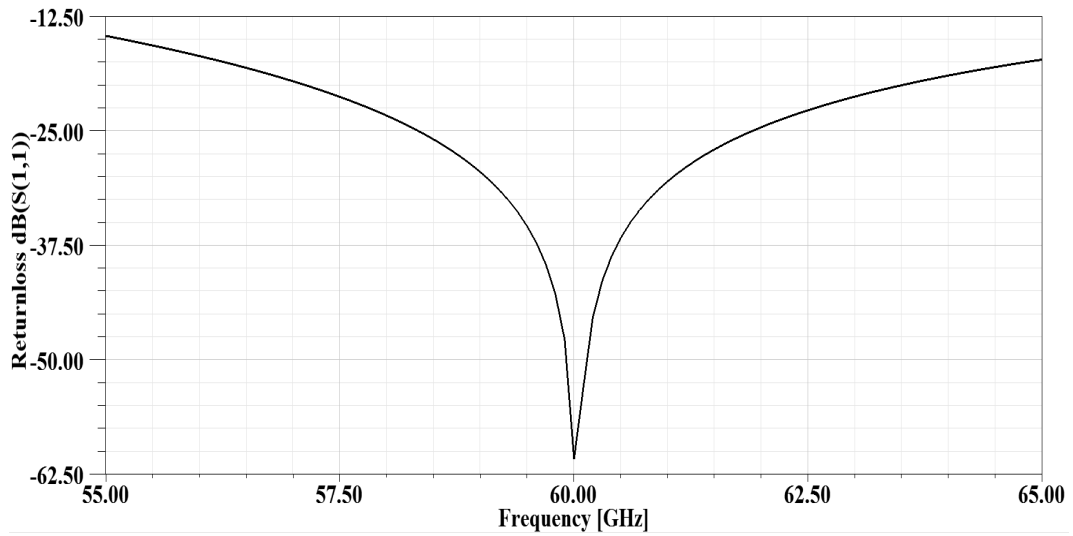


Figure 2.6: Returnloss of Proposed Antenna

From all the plots there exists a good match between theoretically for all the antenna parameters and simulated results. When we compare to previous S-shaped half wave dipole[18] this antenna has more directivity and we can embroider easily on cloths.

## Chapter 3

# Dipole Antenna with N Turns

### 3.1 Introduction

In Chapter 3 we discussed multiturn full-wave dipole antenna with theoretical analysis and HFSS simulation results, main motivation for this work is embroidering the millimetre wave antenna on cloths. Due to insufficient length we can not embroider the 5mm dipole antenna so we need sufficient number of turns for embroidering. We can increase the length of the antenna by increase number of turns N (Each turn length is  $\frac{\lambda}{4}$ ).

As we increase the length of antenna Far-field radiation pattern is different when we compare with full-wave dipole antenna. we are observed radiation patterns and antenna parameters for different lengths. In the straight(linear) dipole antenna radiation pattern is same if we add  $\lambda$  length to half-wave dipole antenna, but in this case for the proposed antenna no same so we were observed radiation patterns for different length. Theoretical Far-field expressions are calculated up to N(=8) turns considering the difficulty in far-field expression calculation. Here we simulated the only symmetrical length and center feed-ed antennas, lengths like multiples of  $\frac{\lambda}{2}$ . In previous chapter we saw far-field patters for full wave dipole antenna. For simulating the antenna we are using High Frequency Structure Simulator(HFSS)

### 3.2 $3\frac{\lambda}{2}$ Dipole antenna

The antenna setup for dipole antenna shown in the below Figure 3.1. As shown in the figure antenna contain N(=6) turns and each turn measurements follows same as we discussed in previous chapter full wave dipole antenna.

#### Current distribution

For the linear dipole antenna current distribution is sinusoidal [22], for the proposed antenna we assumed the current distribution along the antenna is sinusoidal and it is tangential because of antenna position on coordinate axis.

$$I(Z) = I_0 \sin\left(k(H - |Z|)\right), \quad (3.1)$$

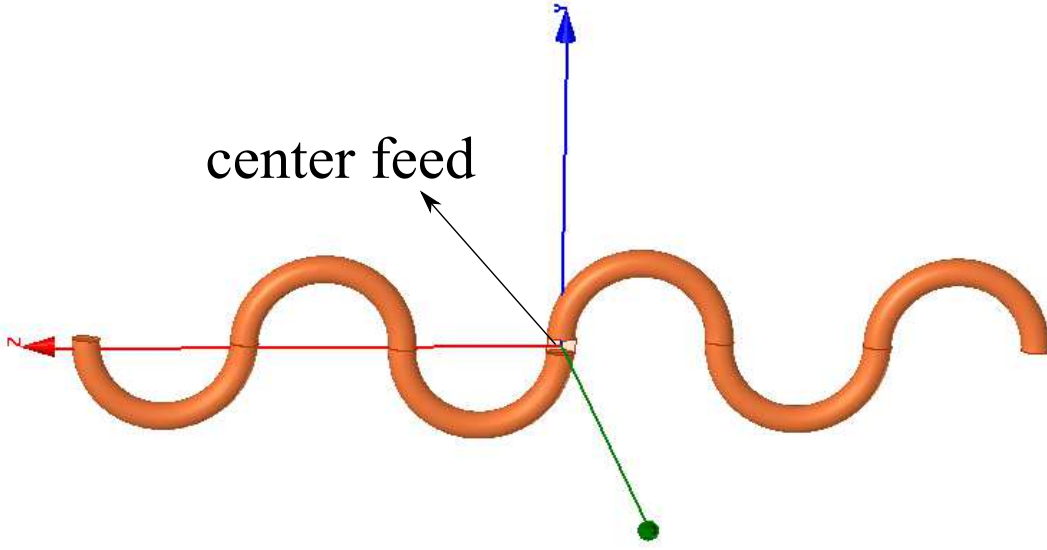


Figure 3.1: Antenna setup

above equation is basic current distribution for the dipole antenna [22]. In the above equation  $H$  is half length of the antenna and  $k$  is wave number. After antenna parameterization as discussed in chapter 3, we have tangential current equations for each turn as shown in below equation.

$$\begin{aligned}
 I_1 &= -I_O \cos(\pi + |kvt|) \hat{a}_y \cos t + \hat{a}_z \sin t, \\
 I_2 &= -I_O \cos(\pi + |kvt|) \hat{a}_y \cos t - \hat{a}_z \sin t, \\
 I_3 &= -I_O \cos(\pi + |kvt|) \hat{a}_y \cos t + \hat{a}_z \sin t, \\
 I_4 &= -I_O \cos(\pi + |kvt|) \hat{a}_y \cos t - \hat{a}_z \sin t, \\
 I_5 &= -I_O \cos(\pi + |kvt|) \hat{a}_y \cos t + \hat{a}_z \sin t, \\
 I_6 &= -I_O \cos(\pi + |kvt|) \hat{a}_y \cos t - \hat{a}_z \sin t.
 \end{aligned} \tag{3.2}$$

### Expressions for Far-Fields

The 2-Step procedure [22] is given in previous chapter for calculating far-fields i.e. finding magnetic vector potential followed by magnetic and electric fields. Calculated magnetic vector potential for each arm in two directions i.e. in Y and Z direction as mentioned in the below equations, calculation procedure is mentioned in previous chapter.

$$\begin{aligned}
 A_{z1} \approx K \left[ -3 \exp(-j\frac{1}{4}(-\sqrt{3} \sin \theta \sin \phi + 9 \cos \theta)) - \right. \\
 \left. \sqrt{3} \exp(-j\frac{1}{4}(-\sqrt{3} \sin \theta \sin \phi + 11 \cos \theta)) \right],
 \end{aligned} \tag{3.3}$$



$$A_{z2} \approx K \left[ -\sqrt{3} \exp(-j\frac{1}{4}(\sqrt{3} \sin \theta \sin \phi + 5 \cos \theta)) - 3 \exp(-j\frac{1}{4}(\sqrt{3} \sin \theta \sin \phi + 7 \cos \theta)) \right], \quad (3.4)$$

$$A_{z3} \approx K \left[ 3 \exp(-j\frac{1}{4}(-\sqrt{3} \sin \theta \sin \phi + \cos \theta)) - \sqrt{3} \exp(-j\frac{1}{4}(-\sqrt{3} \sin \theta \sin \phi + 3 \cos \theta)) \right], \quad (3.5)$$

$$A_{z4} \approx K \left[ \sqrt{3} \exp(-j\frac{1}{4}(\sqrt{3} \sin \theta \sin \phi - 3 \cos \theta)) + 3 \exp(-j\frac{1}{4}(\sqrt{3} \sin \theta \sin \phi - \cos \theta)) \right], \quad (3.6)$$

$$A_{z5} \approx K \left[ -3 \exp(-j\frac{1}{4}(-\sqrt{3} \sin \theta \sin \phi - 7 \cos \theta)) - \sqrt{3} \exp(-j\frac{1}{4}(-\sqrt{3} \sin \theta \sin \phi - 5 \cos \theta)) \right], \quad (3.7)$$

$$A_{z6} \approx K \left[ -\sqrt{3} \exp(-j\frac{1}{4}(\sqrt{3} \sin \theta \sin \phi - 11 \cos \theta)) - 3 \exp(-j\frac{1}{4}(\sqrt{3} \sin \theta \sin \phi - 9 \cos \theta)) \right]. \quad (3.8)$$

$$A_{y1} \approx K \left[ \sqrt{3} \exp(-j\frac{1}{4}(-\sqrt{3} \sin \theta \sin \phi + 9 \cos \theta)) - \exp(-j\frac{1}{4}(-\sqrt{3} \sin \theta \sin \phi + 11 \cos \theta)) + \frac{4}{3} \exp(-j2 \cos \theta) \right]. \quad (3.9)$$

$$A_{y2} \approx K \left[ -\exp(-j\frac{1}{4}(\sqrt{3} \sin \theta \sin \phi + 5 \cos \theta)) + \sqrt{3} \exp(-j\frac{1}{4}(\sqrt{3} \sin \theta \sin \phi + 7 \cos \theta)) + \frac{4}{3} \exp(-j2 \cos \theta) \right]. \quad (3.10)$$

$$A_{y3} \approx K \left[ -\sqrt{3} \exp(-j\frac{1}{4}(-\sqrt{3} \sin \theta \sin \phi + \cos \theta)) + \exp(-j\frac{1}{4}(-\sqrt{3} \sin \theta \sin \phi + 3 \cos \theta)) - \frac{4}{3} \right]. \quad (3.11)$$

$$A_{y4} \approx K \left[ \exp(-j\frac{1}{4}(\sqrt{3} \sin \theta \sin \phi - 3 \cos \theta)) - \sqrt{3} \exp(-j\frac{1}{4}(\sqrt{3} \sin \theta \sin \phi - \cos \theta)) - \frac{4}{3} \right]. \quad (3.12)$$

$$A_{y5} \approx K \left[ \sqrt{3} \exp(-j\frac{1}{4}(-\sqrt{3} \sin \theta \sin \phi - 7 \cos \theta)) - \exp(-j\frac{1}{4}(-\sqrt{3} \sin \theta \sin \phi - 5 \cos \theta)) + \frac{4}{3} \exp(j2 \cos \theta) \right]. \quad (3.13)$$

$$A_{y6} \approx K \left[ -\exp(-j\frac{1}{4}(\sqrt{3} \sin \theta \sin \phi - 11 \cos \theta)) + \sqrt{3} \exp(-j\frac{1}{4}(\sqrt{3} \sin \theta \sin \phi - 9 \cos \theta)) + \frac{4}{3} \exp(j2 \cos \theta) \right]. \quad (3.14)$$

By using maxwell's equations electric and magnetic fields are calculated. Results are plotted by using MATLAB. The following figures shows total electric field at  $\phi = 90^\circ$ . When we observe the Figures 3.2, 4.3 there is close match between theoretical and simulated radiation pattern, so we can confirmed that the antenna has sinusoidal current distribution. The Figure 4.4 shows 3D far-field radiation pattern of  $\frac{3\lambda}{2}$  antenna, it is different from the previous dipole pattern and we can observe side-lobes increases as number of turns increased.

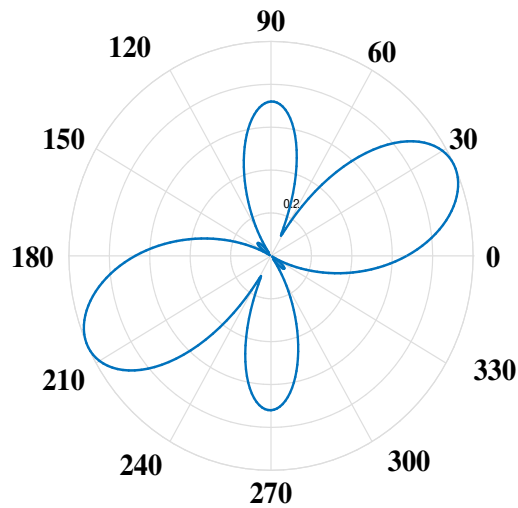


Figure 3.2: Total Electric field (MATLAB)

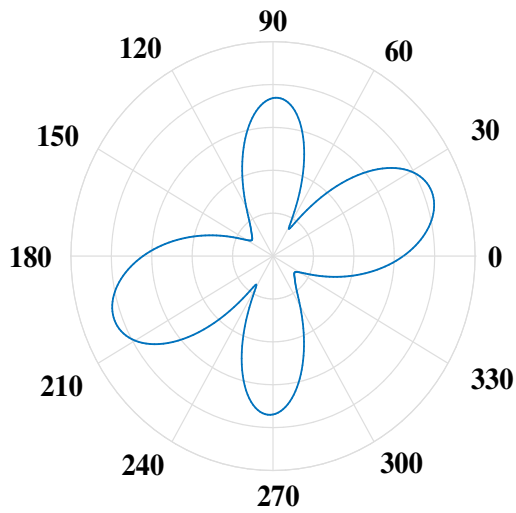


Figure 3.3: Total Electric field (HFSS)

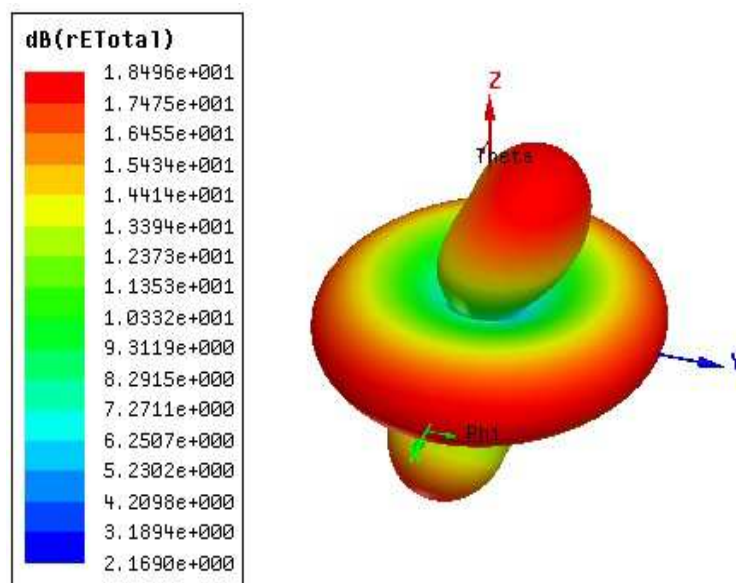


Figure 3.4: 3D polar plot of Total Electric field (HFSS)

### 3.3 $4\frac{\lambda}{2}$ Dipole antenna

Antenna setup is shown in Figure 3.3, in that setup antenna is configured with eight semi-circles, each semi-circle arm measurements mentioned in previous chapter. In this chapter we were observed radiation patterns of different length of embroidery antenna for dipole radiation pattern.

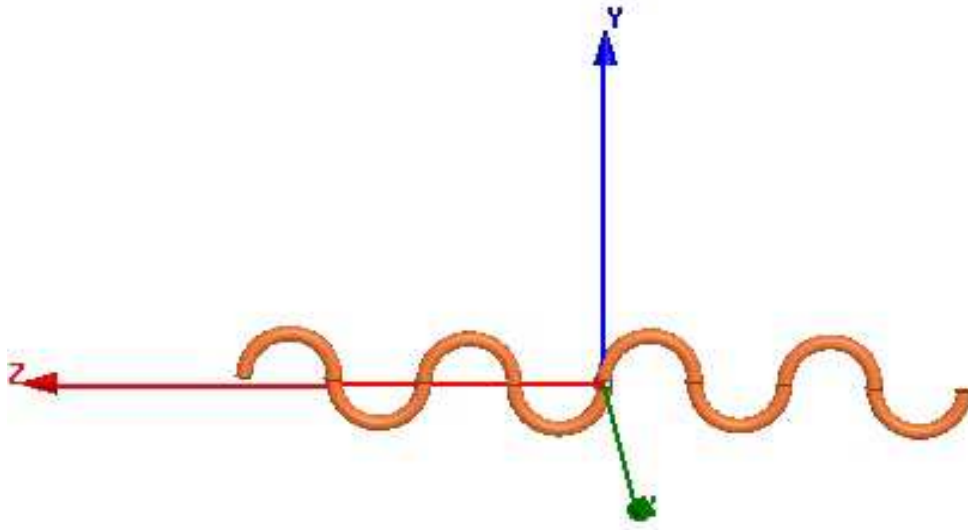


Figure 3.5: Antenna setup

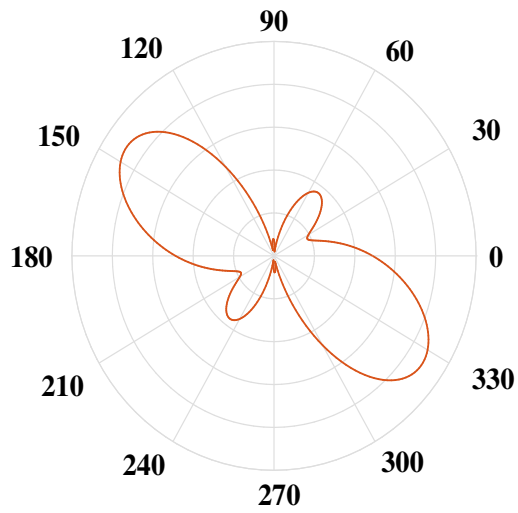


Figure 3.6: Total Electric field (HFSS)

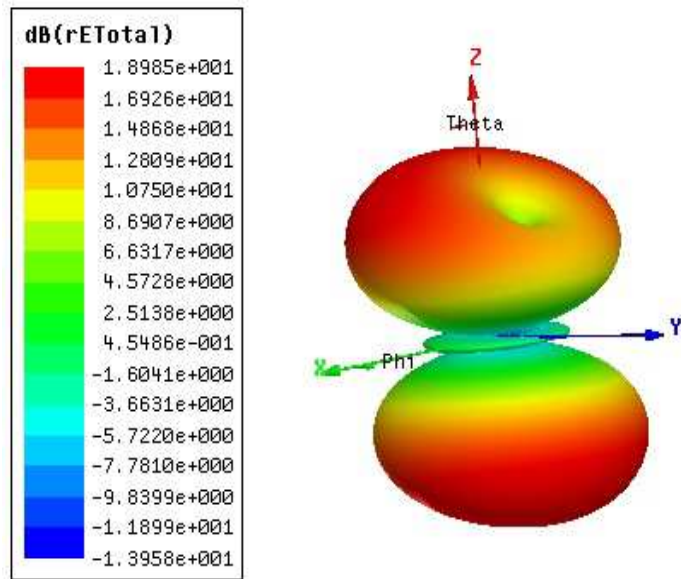


Figure 3.7: 3D polar plot of Total Electric field (HFSS)

### 3.4 $5\frac{\lambda}{2}$ Dipole antenna

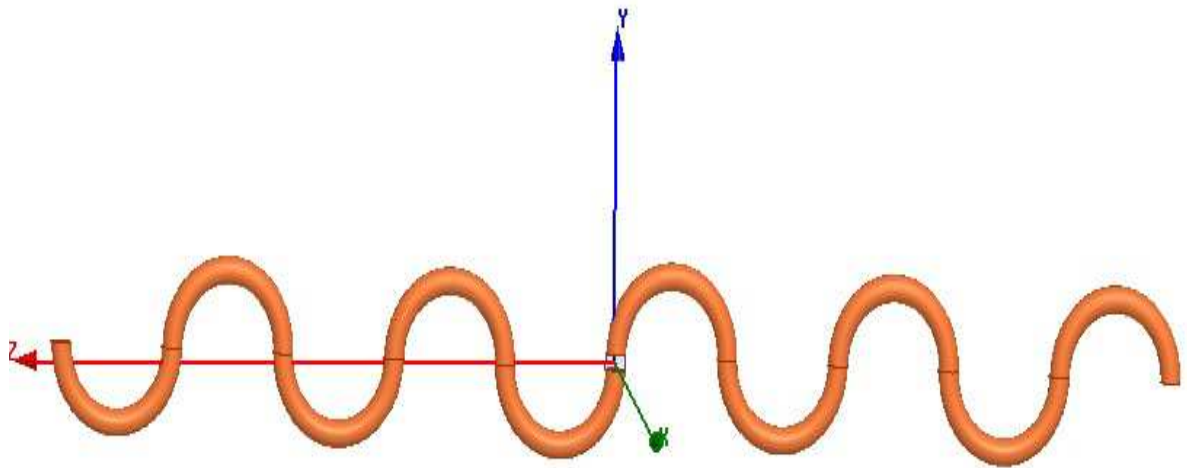


Figure 3.8: Antenna setup

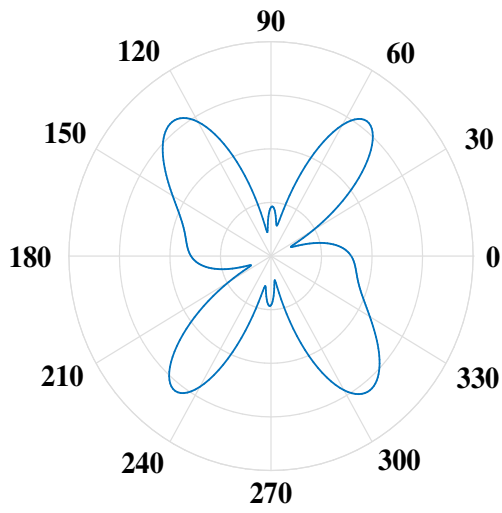


Figure 3.9: Total Electric field (HFSS)

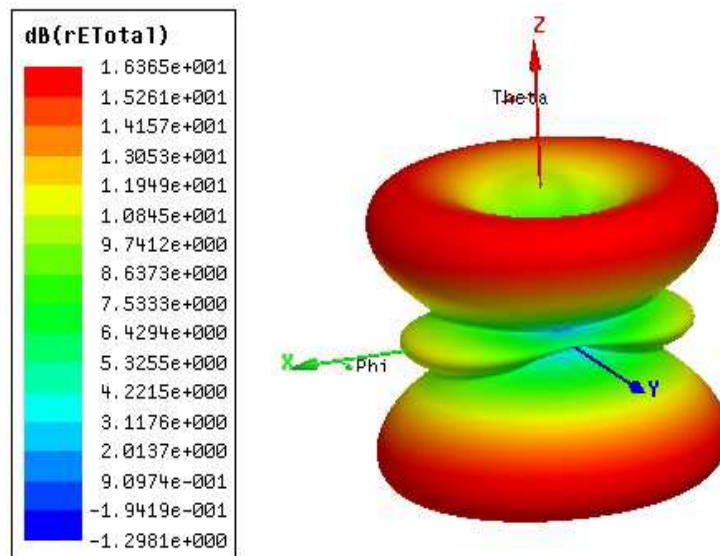


Figure 3.10: 3D Radiation Pattern (HFSS)

### 3.5 $6\frac{\lambda}{2}$ Dipole antenna

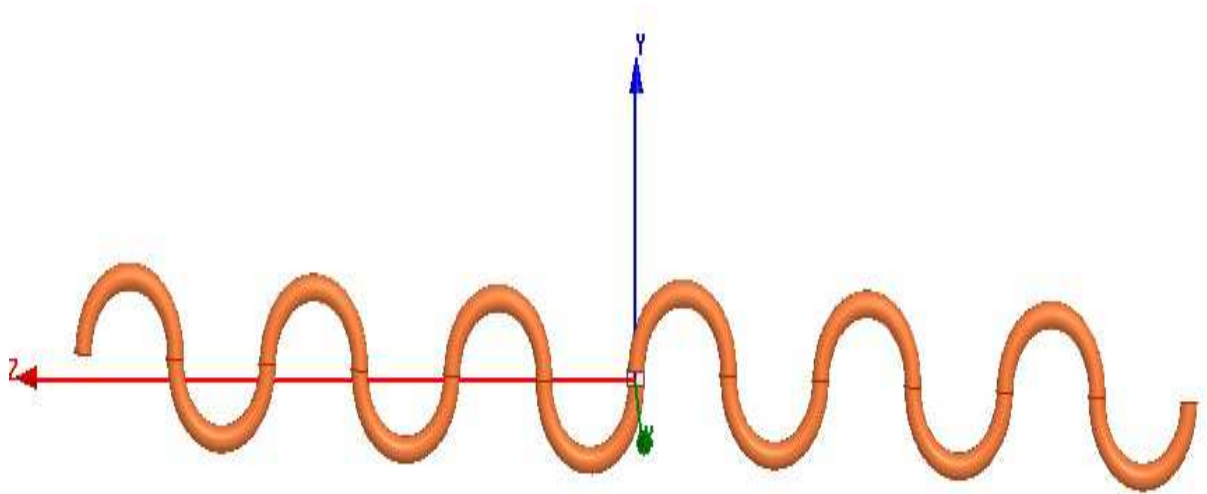


Figure 3.11: Antenna setup

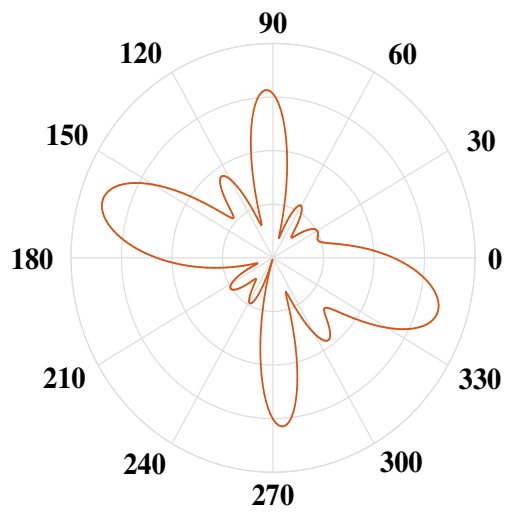


Figure 3.12: Total Electric field (HFSS)

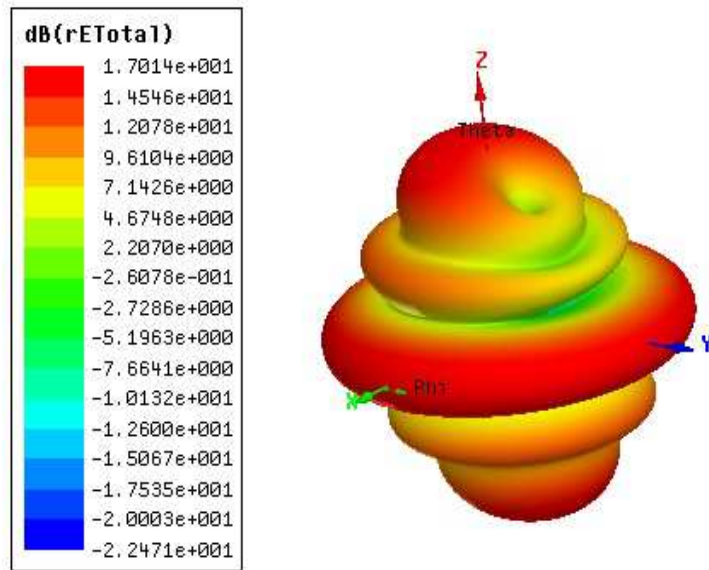


Figure 3.13: 3D Radiation Pattern (HFSS)

### 3.6 $7\frac{\lambda}{2}$ Dipole antenna

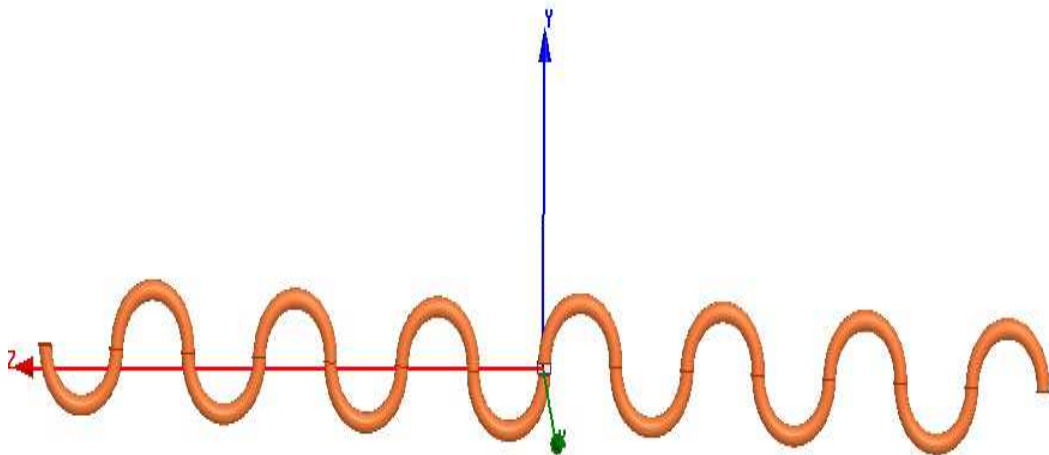


Figure 3.14: Antenna setup



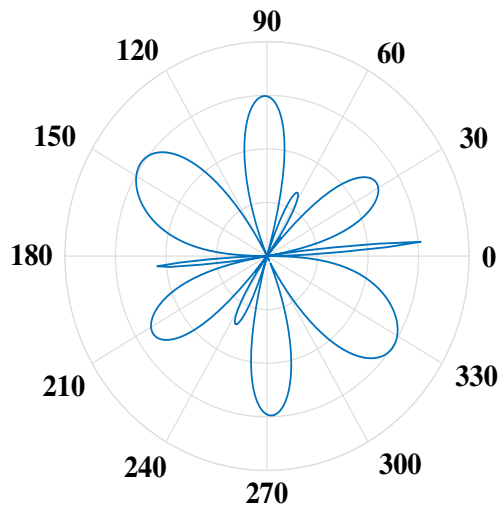


Figure 3.15: Total Electric field (HFSS)

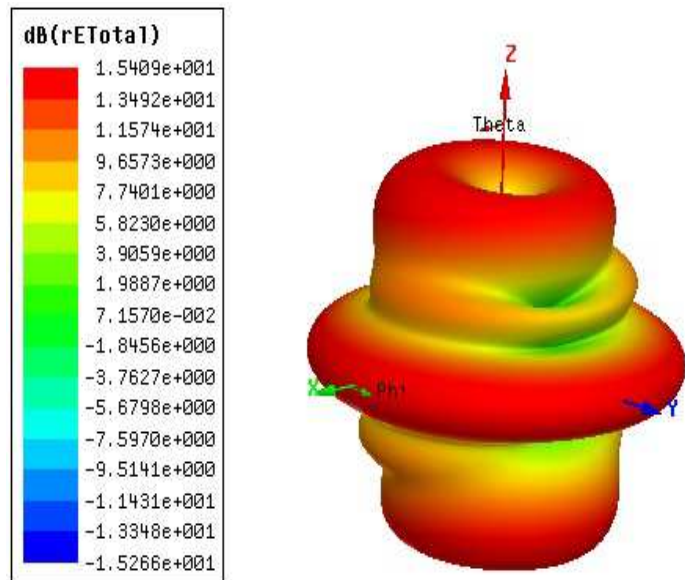


Figure 3.16: 3D Radiation Pattern (HFSS)

### 3.7 $8\frac{\lambda}{2}$ Dipole antenna

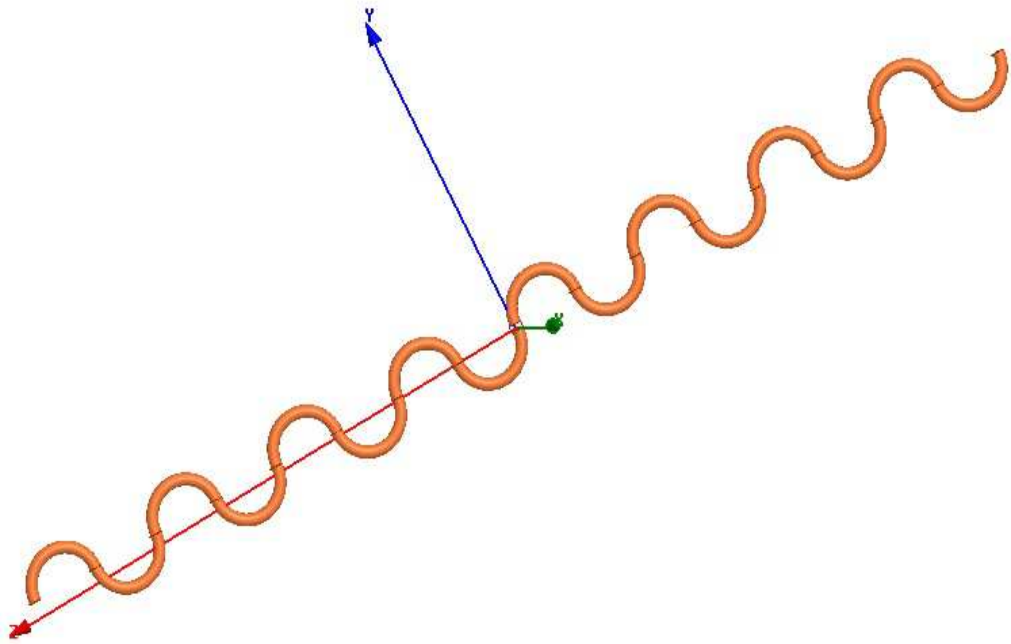


Figure 3.17: Antenna setup

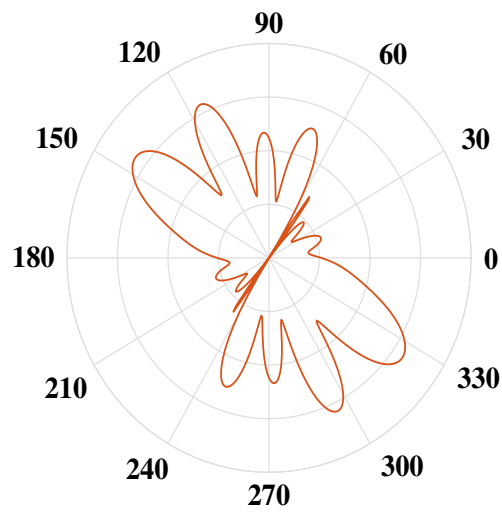


Figure 3.18: Total Electric field (HFSS)

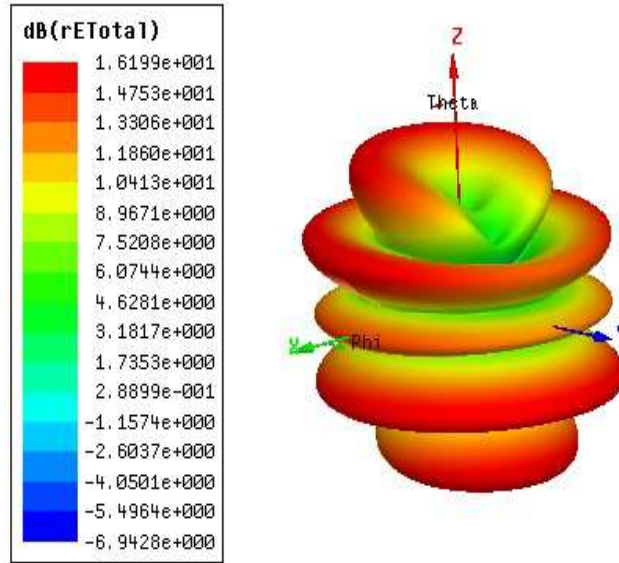


Figure 3.19: 3D Radiation Pattern (HFSS)

### 3.8 Conclusion

Up to  $N(=16)$  turns we observed the far-field radiation patterns and antenna parameters of proposed antenna structures, as  $N$  increases at the far-field power is not concentrated in single direction like dipole, power is wasted in terms of side lobes as shown in above figures. But we have another option like beam forming from antenna arrays. Irrespective of single antenna element radiation pattern we can steer the antenna beam in required direction by using array factor and by changing antenna element excitation phase. Complete details of array construction and excitation phase are discussed in the following chapter.

## Chapter 4

# Millimetre wave Embroidery Beamforming Antenna arrays

### 4.1 Introduction

The wearable communication technology is rapidly growing to enhance quality and efficiency, the devices which support this type of communication need to be small and efficient. The Unlicensed band 57-64 GHz millimetre wave technology promises the wearable on-body and off-body communication, and this spectrum has significant advantages than lower microwave spectrum[25]. This UWB spectrum enable several applications like Telecommunication systems, Health care, Motion tracking, emergency services,medical. The beamforming antennas important in soldier battle field to communicate with soldiers as off-body communication and they need to communicate with devices which are wearable as on-body communication [26]. Patient health care monitoring is advanced with wireless technology and the beamforming arrays enabled communication with several sensor nodes deployed on the patient for monitoring [27],[28].

Developing antennas at millimetre waves is a technological challenge since high accuracy and directivity required [29, 30]. For long distance communication single antenna element insufficient, to ensure that we need to design a beamforming array, this type of arrays can become high directional.

### 4.2 Antenna Array setup

The proposed Antenna array is shown in Figure 4.1(a). The Propose array is designed with N=8 antenna elements, each antenna has  $7\frac{\lambda}{2}$  length. The individual antenna element construction details, current distribution and field equations are discussed in [19, 18]. Each Antenna element is center feed-ed as shown in Figure 4.1(a).  $d$  is the distance between the antenna elements, in this work array results analyzed and compared with  $d = \frac{\lambda}{4}$  and  $\frac{\lambda}{2}$ . The array type is broadside array [31, 22],[32]. The progressive phase shift  $\beta$  [22] between each element can be calculated from equation (1).

$$\beta = kd \cos \theta[22] \tag{4.1}$$

Where  $k$  is wave number  $\frac{2\pi}{\lambda}$ . Beam angle and direction of maximum radiation depends on  $\theta$ . Here the progressive phase shift  $\beta$  is  $0^\circ$ , because  $\theta = 90^\circ$ . When we have embroidered the array on cloth we need the radiation along the perpendicular to antenna axis as shown in Figure 4.4, so to ensure that we selected the  $\theta = 90^\circ$ . We can steer the beams in required direction depends on  $\theta$ .

### 4.3 Antenna array with Reflector

The Proposed array has all dipole antenna elements, so we get radiation in all directions as shown in Figure 4.4(a).when we embroidered the antenna on cloth we need to reduce the effect of electromagnetic radiation towards the human body to ensure that here we are used a copper sheet as reflector is shown in Figure 4.1(b). Side view of array setup with reflector is shown in Figure 4.1(c), here we consider the minimum distance between the antenna array and reflector is  $\frac{\lambda}{4}$  [22]. Reflectors also reducing the signals received from back side of the antenna. By adding reflector to the array, the gain of the array further improved and we can get more directional beams.

The radiation patterns with and without reflector are shown in Figure 4.4, the reflected field is add with front field and gives strong beams in the direction of perpendicular to antenna axis as shown in Figure 4.4. Due to placed the reflector behind the antenna array 20 dB (approx.) gain reduced in the required direction.

## 4.4 Antenna Parameters

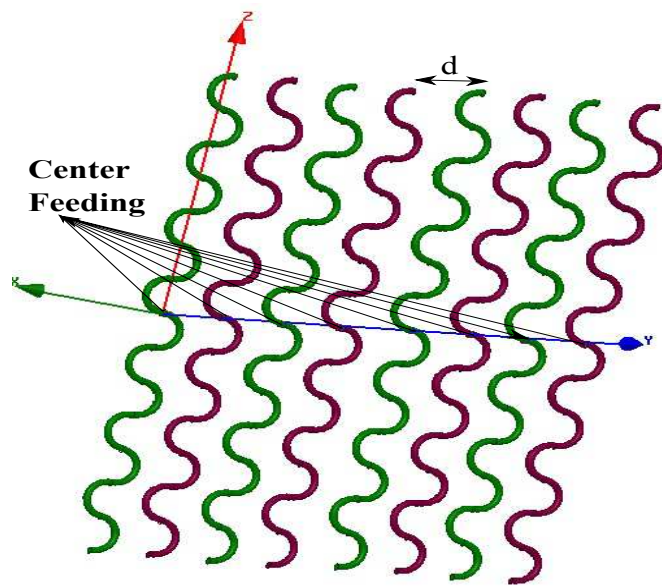
### 4.4.1 Directivity and Gain

The Directivity of an antenna is defined as the ratio of the radiation intensity in a given direction to the radiation intensity averaged over all directions. For this array, total directivity is 11dB along  $\theta = 90^\circ$  direction. The total gain for proposed antenna array shown in Figure 4.2 and gain comparisons for radiated beams of different type of antenna elements are shown in the table when we compared to single antenna element the proposed antenna array with reflector is getting high gain beams. This high directive and high gain array beams are used to cover smaller areas [33] in outdoor communication like in battle field for soldier communications [26] and indoor communication like in the hospital for monitoring patient health condition [27].

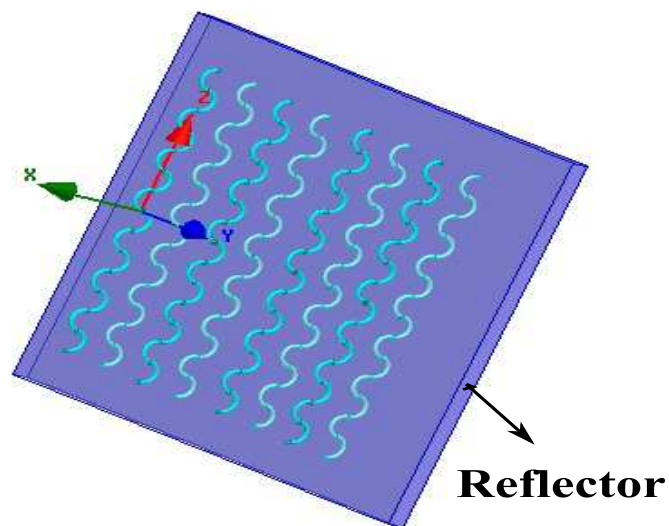
### 4.4.2 Radiated Electric field

The 3D plot of the Magnitude of total electric field is shown in Figure 4.4. Strong beams are forming in the direction of  $\phi = 90^\circ$  and  $\phi = 270^\circ$  that is shown in Figure 4.4(a). By using the reflector we can steer the radiated beams required direction with negligible sidelobe power, as shown in the Figure 4.4(b). As the distance between the elements increases the beam width decreases in the direction of  $\phi$ . This narrow beam width allows accurate targeting of the radio signals in the required direction.

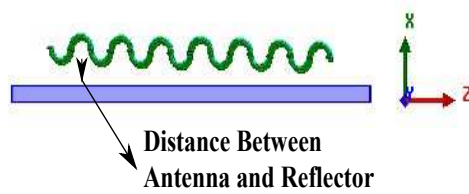
S.NO	Type	Gain(dB)\Beam1	Beam2	Beam3
1	Single Element	3.5	5.4	4.3
2	Array	9.5	11.4	9.5
3	Array with Reflector	9.8	11	13



(a) Array without reflector



(b) Array with reflector



(c) Array with reflector

Figure 4.1: Array Setup

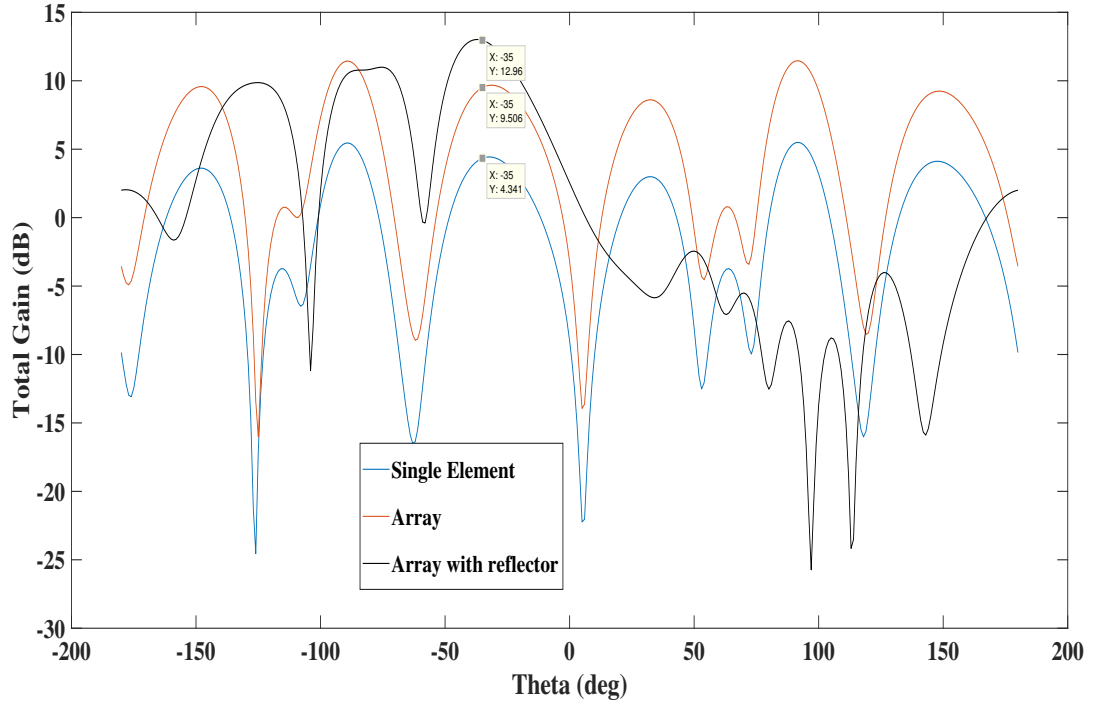


Figure 4.2: Total Gain Comparison

#### 4.4.3 Return losses and Mutual coupling

Return loss is the important parameter for antenna design, it measures how much power return to antenna port due to mismatch with the transmission line.  $S_{ij}$  represents the return loss when  $i = j$  else it represents mutual coupling between antenna elements. The proposed antenna array is designed such that,

$$S_{ij} < -10\text{dB}; \text{ for } i = j \quad (4.2)$$

Figure 4.5(a) shown the return loss of proposed array, each antenna element in the array resonates at 60GHz, and the array occupies entire bandwidth 57-63GHz for antenna element distance  $\frac{\lambda}{4}$ . When the distance between elements increased to  $\frac{\lambda}{2}$  then the operating band width reduced as shown in Figure 4.5(b), the occupied bandwidth is 57.8 - 61.2GHz.

Mutual coupling is the electromagnetic interaction between the antenna elements in the array, due to mutual coupling current distribution, input impedance and array far field radiation pattern gets effected. As the distance between the antenna elements in the array increases then the mutual coupling decreases [22].

#### 4.4.4 Antenna feeding and impedance Matching

In the proposed array all the antenna elements are center feed-ed [19, 22], we can choose off centre feed-ed antenna elements to make sure that current will not be equal to zero at the feed point of the antenna element.

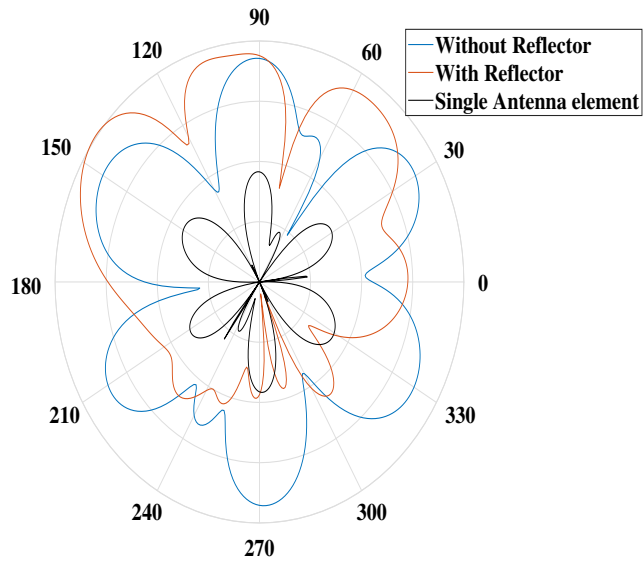


Figure 4.3: Electric Field comparison ( $\phi = 90^\circ$ )

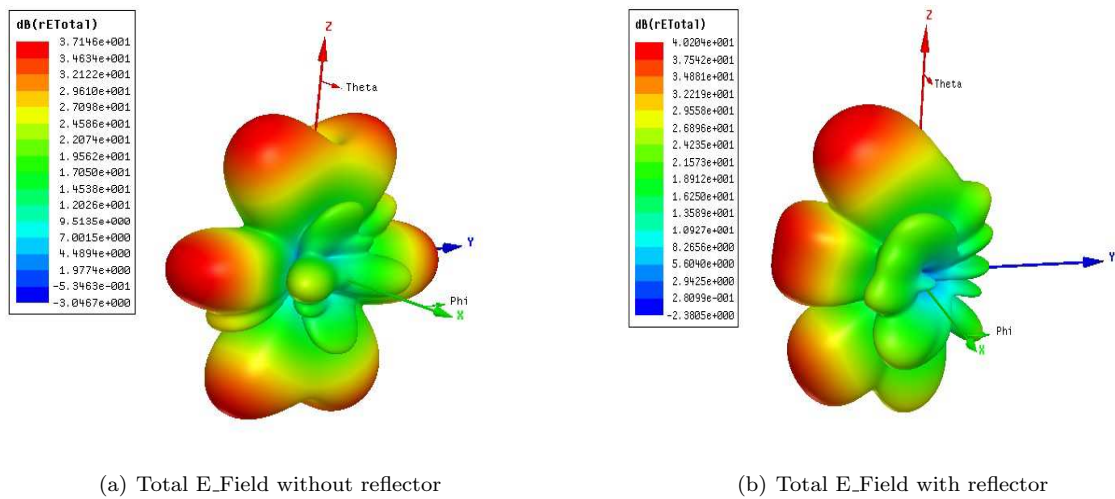
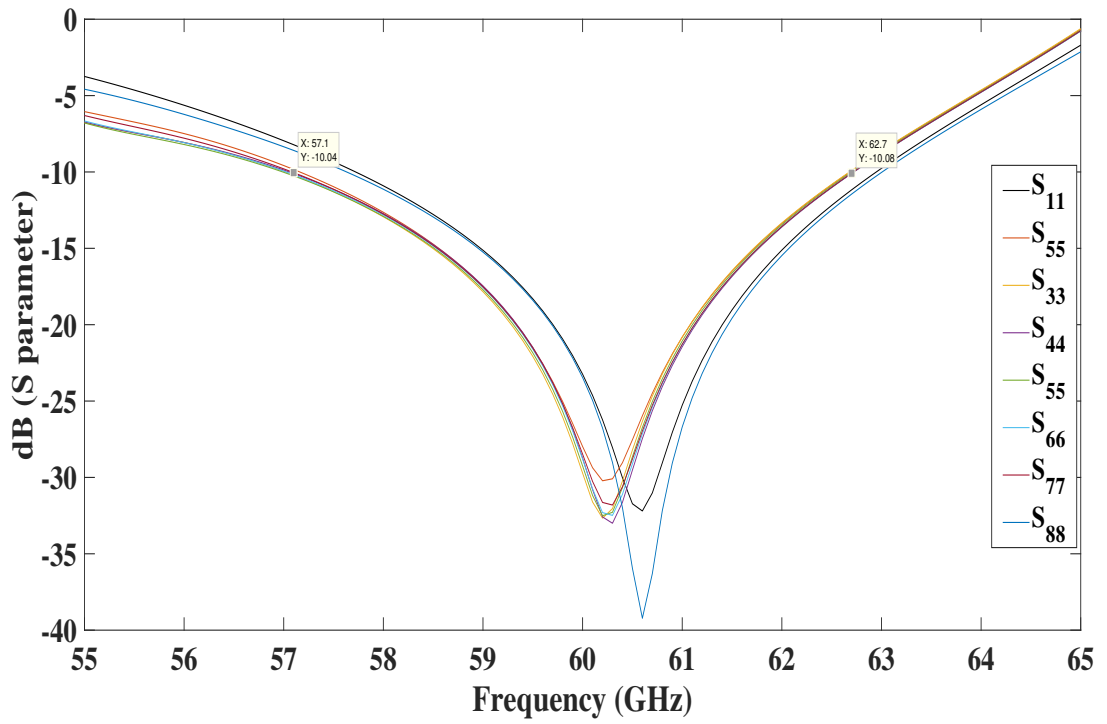
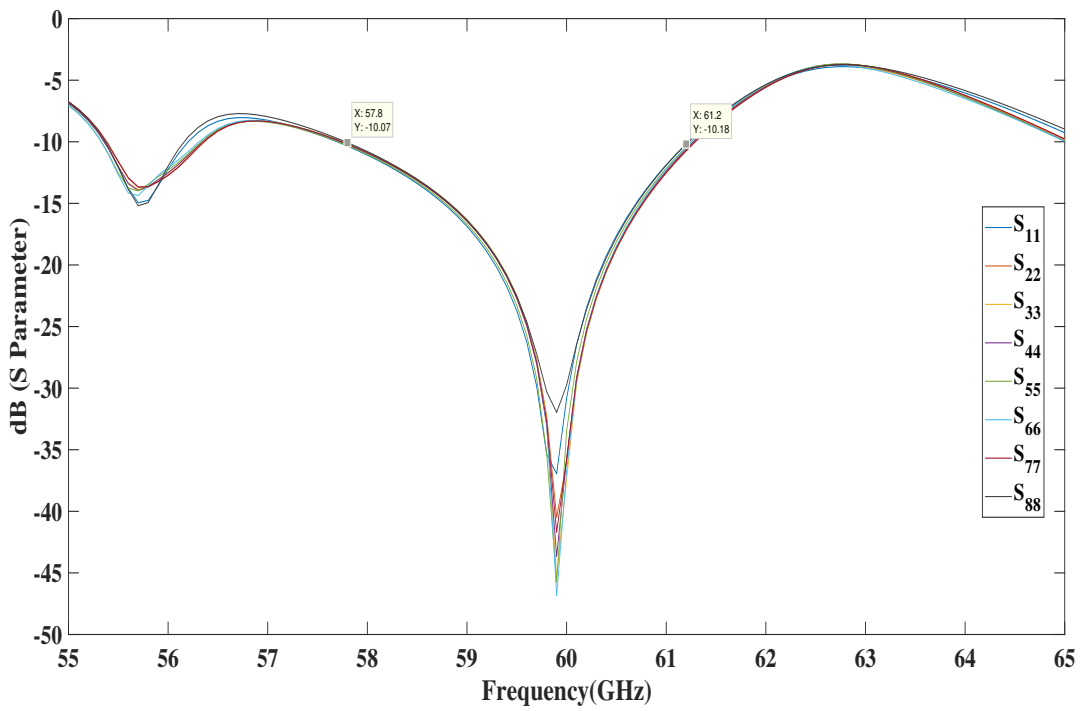


Figure 4.4: Electric Field





(a)



(b)

Figure 4.5: Return losses

Antenna array input impedance for different distances between antenna elements shown in Figure 6. Due to mutual coupling between the elements, the input impedance of both extreme end antenna elements gets effected that we can observe in Figure 6(a). As the distance between antenna elements increases all the antenna elements have the same input impedance (approx.) as shown in Figure 6(b). For antenna array resonance we need to match the array input impedance with excitation. So for the input impedance matching, we can follow the technique is discussed in [19].

## 4.5 Limitation on number of Antenna Elements and length

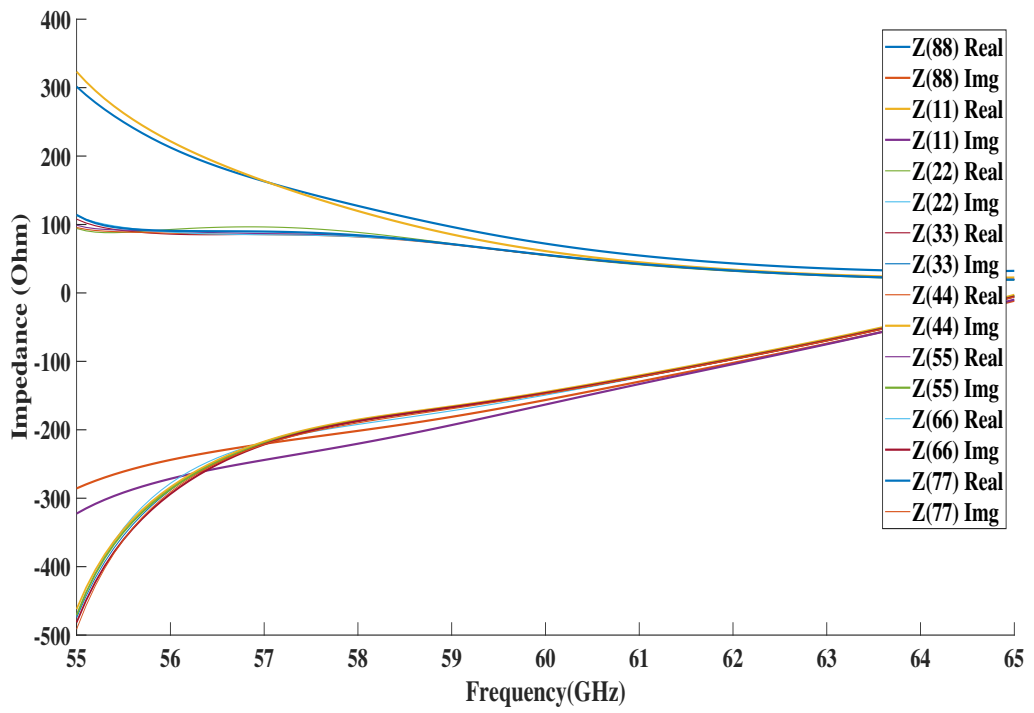
All the above simulation results are shown for  $N (= 14)$  antenna elements and length of each antenna element is  $7\frac{\lambda}{2}$ , if each antenna element length, increase at constant  $N (= 14)$  then the side lobes increases and the radiated power wasted as side lobes. At constant element length if we can increase  $N$ , there is no wastage of radiated power in side lobes. The total electric field is shown in Figure 4(a). So each antenna element length  $7\frac{\lambda}{2}$  is highly recommended for antenna array to get strong beams.

S.NO	Type	Measurement
1	Number of turns	14
2	Length of copper wire	17.5mm
3	Diameter of copper wire	0.2-0.5mm
4	Diameter of each turn	0.8mm
5	Distance between each antenna element	1.25-2mm

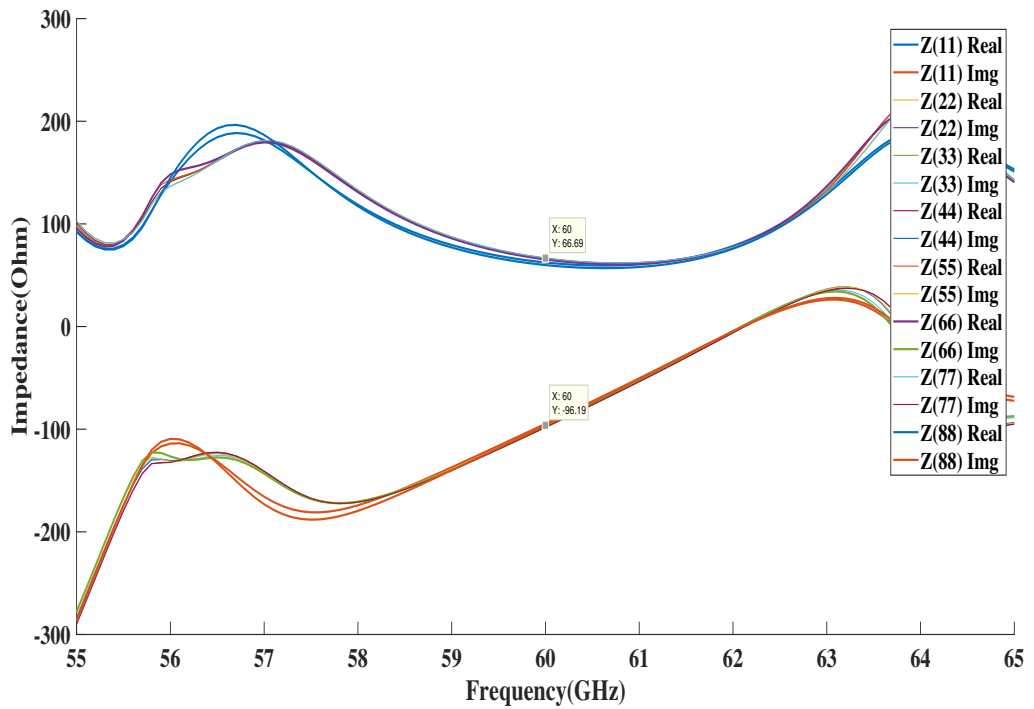
## 4.6 Conclusion and Future work

For millimetre wavelengths beam forming antennas play a key role in communication, the proposed antenna arrays form strong beams in the required direction. The Structure of antenna element gives us a big advantage, it can be easily embroidered on cloths. When we compare with planar antennas the proposed structures can be easily positioned on clothes. By incorporating this type of antenna array devices the size of operating system significantly reduced.

Side lobes are main reason for radiated power wastage to prevent that side lobe power we have several techniques like amplitude tampering and adaptive beam forming algorithms, we can apply these algorithms on proposed antenna array structure.



(a)  $\frac{\lambda}{4}$  distance between elements



(b)  $\frac{\lambda}{2}$  distance between elements

Figure 4.6: Antenna array Input impedance

# References

- [1] B. Langen, G. Lober, and W. Herzig. Reflection and transmission behaviour of building materials at 60 GHz. In 5th IEEE International Symposium on Personal, Indoor and Mobile Radio Communications, Wireless Networks - Catching the Mobile Future. 1994 505–509 vol.2.
- [2] N. Guo, R. C. Qiu, S. S. Mo, and K. Takahashi. 60-GHz millimeter-wave radio: Principle, technology, and new results. *EURASIP journal on Wireless Communications and Networking* 2007, (2007) 48–48.
- [3] C. Park and T. S. Rappaport. Short-range wireless communications for next-generation networks: UWB, 60 GHz millimeter-wave WPAN, and ZigBee. *IEEE Wireless Communications* 14.
- [4] pinterest, <https://in.pinterest.com/pin/639370478319838075/>.
- [5] R. Fisher. 60 GHz WPAN standardization within IEEE 802.15. 3c. In Signals, Systems and Electronics, 2007. ISSSE'07. International Symposium on. IEEE, 2007 103–105.
- [6] P. S. Hall and Y. Hao. Antennas and propagation for body centric communications. In 2006 First European Conference on Antennas and Propagation. 2006 1–7.
- [7] A. Pellegrini, A. Brizzi, L. Zhang, K. Ali, Y. Hao, X. Wu, C. C. Constantinou, Y. Nechayev, P. S. Hall, N. Chahat, M. Zhadobov, and R. Sauleau. Antennas and Propagation for Body-Centric Wireless Communications at Millimeter-Wave Frequencies: A Review [Wireless Corner]. *IEEE Antennas and Propagation Magazine* 55, (2013) 262–287.
- [8] X. Lin, B.-C. Seet, and F. Joseph. Fabric antenna with body temperature sensing for BAN applications over 5G wireless systems. In Sensing Technology (ICST), 2015 9th International Conference on. IEEE, 2015 591–595.
- [9] N. Chahat, G. Valerio, M. Zhadobov, and R. Sauleau. On-Body Propagation at 60 GHz. *IEEE Transactions on Antennas and Propagation* 61, (2013) 1876–1888.
- [10] S. Alipour, F. Parvaresh, H. Ghajari, and F. K. Donald. Propagation characteristics for a 60 GHz Wireless body area network (WBAN). In 2010 - MILCOM 2010 MILITARY COMMUNICATIONS CONFERENCE. 2010 719–723.
- [11] M. Zhadobov, N. Chahat, R. Sauleau, C. Le Quement, and Y. Le Drean. Millimeter-wave interactions with the human body: state of knowledge and recent advances. *International Journal of Microwave and Wireless Technologies* 3, (2011) 237247.

- [12] C. Gustafson and F. Tufvesson. Characterization of 60 GHz shadowing by human bodies and simple phantoms. In 2012 6th European Conference on Antennas and Propagation (EUCAP). 2012 473–477.
- [13] S. Alipour, F. Parvaresh, H. Ghajari, and F. Donald. Propagation characteristics for a 60 GHz Wireless body area network (WBAN). *2010 - MILCOM 2010 MILITARY COMMUNICATIONS CONFERENCE* 719–723.
- [14] <http://www.cwins.wpi.edu/personnel/guanqun/index.html>.
- [15] P. Salonen, L. Sydanheimo, M. Keskilammi, and M. Kivikoski. A small planar inverted-F antenna for wearable applications. In Digest of Papers. Third International Symposium on Wearable Computers. 1999 95–100.
- [16] X. Y. Wu, L. Akhoondzadeh-Asl, Z. P. Wang, and P. S. Hall. Novel Yagi-Uda antennas for on-body communication at 60GHz. In 2010 Loughborough Antennas Propagation Conference. 2010 153–156.
- [17] N. Chahat, M. Zhadobov, and R. Sauleau. Wearable textile patch antenna for BAN At 60 GHz. In 2013 7th European Conference on Antennas and Propagation (EuCAP). 2013 217–219.
- [18] S. Channa, L. Panwar, S. R. K. Vanjari, and M. Z. A. Khan. A S-shaped millimeter wave antenna for UWB applications. In 2017 Progress In Electromagnetics Research Symposium - Spring (PIERS). 2017 484–489.
- [19] D. A. Kumar and M. Z. A. Khan. An embroidered millimeter full wave dipole antenna for UWB applications. In 2017 Progress in Electromagnetics Research Symposium - Fall (PIERS - FALL). 2017 2617–2624.
- [20] Y. Li and K. M. Luk. A Multibeam End-Fire Magnetolectric Dipole Antenna Array for Millimeter-Wave Applications. *IEEE Transactions on Antennas and Propagation* 64, (2016) 2894–2904.
- [21] P. Nepa and G. Manara. Design and characterization of wearable antennas. In Electromagnetics in Advanced Applications (ICEAA), 2013 International Conference on. IEEE, 2013 1168–1171.
- [22] C. A. Balanis. Antenna theory: analysis and design. John Wiley & Sons, 2016.
- [23] R. King and C. Harrison. The distribution of current along a symmetrical center-driven antenna. *Proceedings of the IRE* 31, (1943) 548–567.
- [24] K. Sakakibara, M. Ikeda, T. Suzuki, W. Maeda, K. Ookawa, Y. Aoki, N. Kikuma, and H. Hirayama. Layer-structured detector module for passive millimeter-wave imaging. In Microwave Conference, 2009. EuMC 2009. European. IEEE, 2009 1630–1633.
- [25] N. Chahat, M. Zhadobov, L. L. Coq, and R. Sauleau. Wearable Endfire Textile Antenna for On-Body Communications at 60 GHz. *IEEE Antennas and Wireless Propagation Letters* 11, (2012) 799–802.
- [26] N. Chahat, M. Zhadobov, and R. Sauleau. Antennas for body centric wireless communications at millimeter wave frequencies. In Progress in compact antennas. InTech, 2014.

- [27] P. J. Soh, B. V. den Bergh, H. Xu, H. Aliakbarian, S. Farsi, P. Samal, G. A. E. Vandenbosch, D. M. M. P. Schreurs, and B. K. J. C. Nauwelaers. A smart wearable textile array system for biomedical telemetry applications. *IEEE Transactions on Microwave Theory and Techniques* 61, (2013) 2253–2261.
- [28] A. R. Guraliuc, N. Chahat, C. Leduc, M. Zhadobov, and R. Sauleau. End-Fire Antenna for BAN at 60 GHz: Impact of Bending, On-Body Performances, and Study of an On to Off-Body Scenario. *Electronics* 3, (2014) 221–233.
- [29] D. M. Pozar, S. D. Targonski, and H. D. Syrigos. Design of millimeter wave microstrip reflectarrays. *IEEE Transactions on Antennas and Propagation* 45, (1997) 287–296.
- [30] C.-H. Tseng, C.-J. Chen, and T.-H. Chu. A low-cost 60-GHz switched-beam patch antenna array with Butler matrix network. *IEEE Antennas and Wireless Propagation Letters* 7, (2008) 432–435.
- [31] I. J. Chen, Y. C. Tseng, and T. L. Wu. Beamforming broadside antenna array for 60-GHz technology. In 2016 IEEE International Symposium on Radio-Frequency Integration Technology (RFIT). 2016 1–3.
- [32] I. J. Chen, Y. C. Tseng, and T. L. Wu. Beamforming broadside antenna array for 60-GHz technology. In 2016 IEEE International Symposium on Radio-Frequency Integration Technology (RFIT). 2016 1–3.
- [33] S. Hur, T. Kim, D. J. Love, J. V. Krogmeier, T. A. Thomas, and A. Ghosh. Millimeter Wave Beamforming for Wireless Backhaul and Access in Small Cell Networks. *IEEE Transactions on Communications* 61, (2013) 4391–4403.

# Appendix A

## High Frequency Structure Simulator

### A.1 Introduction

ANSYS High frequency Structure Simulator(HFSS) is a standard used for simulating high frequency electromagnetic fields. HFSS is a simulation tool for complex 3D geometry. It is one of the commercial design tool for antenna design, transmission lines and RF circuits.

### A.2 Mathematical method used by HFSS

The numerical technique Finite element method one of the best method to solve complex geometry with negligible errors. In this procedure the structure which we want to simulate is divided into small parts. These small parts are called tetrahedrons. Technically these structure partition(entire collection of tetrahedral) is called meshing. For the fields a solution is found in each finite element and these solutions are interrelated so that maxwell equations are satisfied across inter element boundaries. So that finally it yields one solution for entire structure and after that it found generalized S parameter matrix.

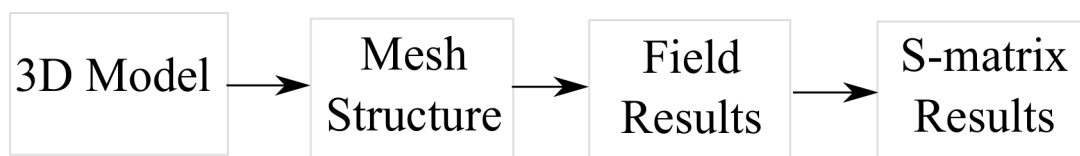


Figure A.1: HFSS solution procedure

#### A.2.1 Adaptive solution

Adaptive solution is a mathematical iterative process used by HFSS and it gives high accuracy solution to a give Electro magnetic field problm.

Following steps are followed by Adaptive analysis.

- Generating initial mesh structure
- HFSS computes the electromagnetic field inside the structure when it is excited at the solution frequency. In this work solution frequency is 60GHz and the frequency sweep is 57-64GHz.
- Based on current finite solution HFSS find the tetrahedron region where the error is high. In this region mesh is refined for the error converge.
- It generates another solution for refined mesh.
- Again it calculate the error. Iterative process(solution- $\rightarrow$  error analysis- $\rightarrow$  refine mesh) is running until error converges or adaptive passes completed. (In this work all simulations completed with 0.02 error convergence and 6 adaptive passes).
- If we consider frequency sweep same above process taken at every frequency point without refine the mesh.

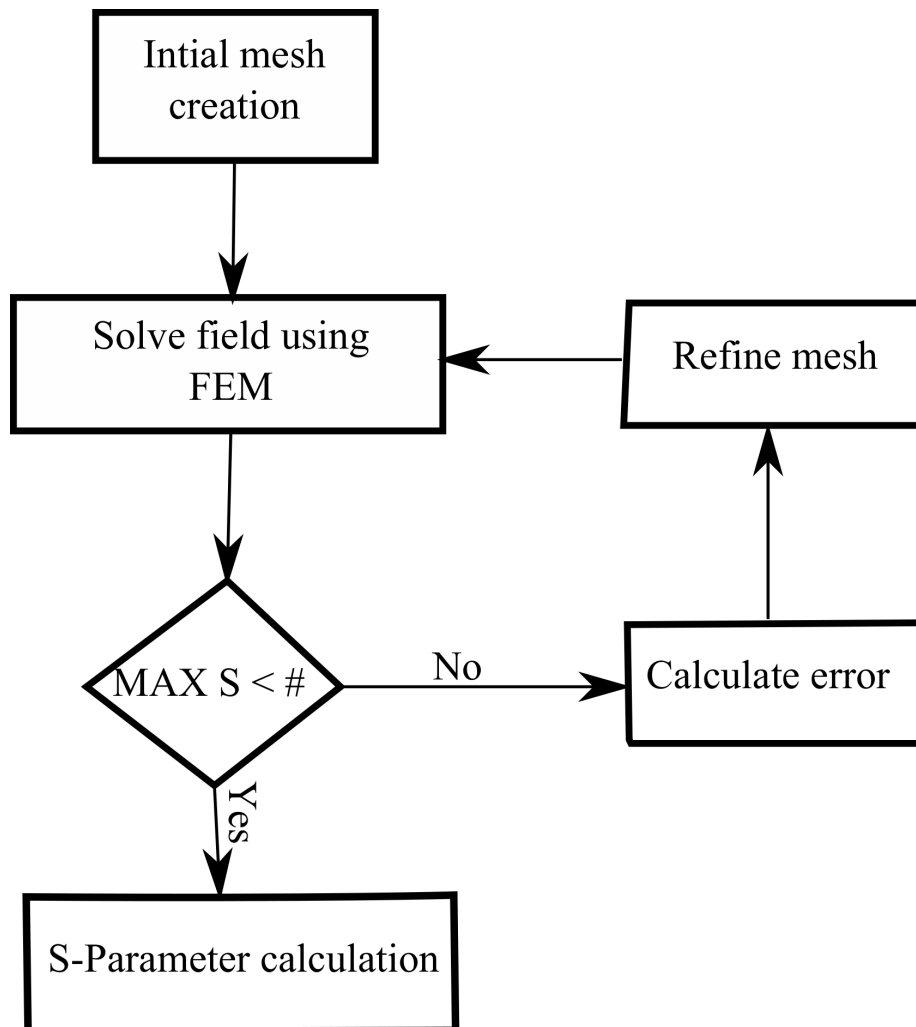


Figure A.2: Adaptive Pass procedure



### A.3 Steps followed in HFSS simulation

There are six steps we need to follow proper HFSS simulation

- **Create geometry**

The first task is creating HFSS model i.e. the physical model that a user wants to analyze. The model can be create using HFSS 3D modeler and it is fully parametric and enables user create structure. we can import structures from the Solid works, Auto cad and PRO-E. The imported structures are not parameterized and user can not change in HFSS 3D modeler. In this work we are create Antenna using HFSS 3D modeler.

- **Assign boundaries**

The main purpose of assign boundaries are to create closed/open electromagnetic models and to simplify complexity of the electromagnetic model. In HFSS there are twelve boundaries. In this work we are using only radiation boundary because the created antenna model is open model. Open model represents the electromagnetic energy within the model is radiate away. Radiation boundary applied to the outer faces of solution space and it should be placed quarter wavelength away from the antenna.

- **Assign Excitation**

IN HFSS there are different types of Excitations like fields, current and voltage. User need to specify an excitation to simulating model. In this work all the simulations are done with Lumped port. This port provides field information as well as S,Y,Z parameters.

- **Solution setup**

In the solution setup the desirable parameters are frequency and delta-s. The solution frequency nothing but operating frequency at which simulating model need to be analyzed. In this work all simulations done at 60GHz and maximum delta-s is 0.02 i.e. error percentage. Error should be converged within adaptive passes completed.

- **Solve**

After done with initial four steps we ae ready with the model for analyze. Time required for the analyzing the given model is depending on solution frequency and error convergence percentage.

- **Post processing results**

In post processing we are examine the S-parameters and plotting the far-fields around the given antenna structure. In this work we are mainly focused on return losses of antenna and design antenna such that it creates Beam forming fields in the required direction.

S.NO	Type	HFSS
1	Material used for design	Copper wire
2	Solution Frequency	60GHz
3	Frequency sweep	57-64GHZ
4	No of adaptive passes	6
5	Error convergence	0.02
6	Boundary	Radiation
7	Excitation port	Lumped Port

## A.4 Materials and Dimensions

In this work for Antenna design high conductivity copper wire is used. Dimensions like length and diameter of the wire selected according to solution frequency. Diameter of copper wire is selected as less than  $\frac{\lambda}{10}$  [22]. Here  $\lambda$  is wavelength i.e. 5mm. In the following chapter 5 we are designed antenna arrays, in the design for beam steering reflector was used. For reflector 0.5mm copper sheet was used.